Marine Pollution Bulletin 223 (2026) 118969

Contents lists available at ScienceDirect

Marine Pollution Bulletin

journal homepage: www.elsevier.com/locate/marpolbul

Tracing threats across the land–marine transition areas: Decoding heavy metal sources and risks in soil-water-sediment systems of northern and eastern coastal China

Qiumei Wu [a,b,c], Peng Liu [d], Shiyi Zhang [a], Guojing Yan [a], Kang Tian [a], Wenyou Hu [a,b,*], Tieyu Wang [e], Jong Seong Khim [f], Seongjin Hong [g], Bong-Oh Kwon [h], Ya''nan Fan [a], Biao Huang [a,b]

[a] State Key Laboratory of Soil and Sustainable Agriculture, Institute of Soil Science, Chinese Academy of Sciences, Nanjing, 211135, China
[b] Sino-Danish College, University of Chinese Academy of Sciences, Beijing, 100049, China
[c] Sino-Danish Center for Education and Research (SDC), Beijing, 100049, China
[d] College of Resources and Environment, Anqing Normal University, Anqing, 246011, China
[e] Institute of Marine Sciences, Shantou University, Shantou, 515063, China
[f] School of Earth and Environmental Sciences, Research Institute of Oceanography, Seoul National University, Seoul, 08826, Republic of Korea
[g] Department of Marine Environmental Sciences, Chungnam National University, Daejeon, 34134, Republic of Korea
[h] Department of Marine Biology, Kunsan National University, Kunsan, 54150, Republic of Korea

ARTICLE INFO

Keywords:
Coastal environment
Geochemical baseline
Heavy metals
Isotopic tracing
Potential ecological risk

ABSTRACT

Heavy metal(loid)s (HMs) in coastal environments exhibit complex cross-media transport and ecological risks under the combined influence of natural and anthropogenic processes. This study conducted a comprehensive tri-media (soil, water, and sediment) assessment in a typical coastal area of northern and eastern China. The study integrated geochemical baselines (GeoBs), source apportionment, partitioning behavior, and ecological risk prediction. GeoBs of cadmium (Cd) and lead (Pb) in both soil and sediment exceeded regional background levels. 22.55 % of the sampling sites for Cd and 28.43 % for Pb were located within the dual-media pollution zone. PMF analysis indicated two main source categories: lithogenic inputs (Cr, Ni) contributed 46.2 % in sediment and 50.9 % in soil, while anthropogenic activities (agriculture, industry, atmospheric deposition) accounted for 37–41 %. Pb isotope ratios ($^{206}Pb/^{207}Pb = 1.17 \pm 0.013$) in surface soils overlapped with signatures from factory and vehicular emissions. Cd isotope analysis showed that about 56 % of Cd in surface soils originated from anthropogenic inputs, with 44 % derived from parent material. Partition coefficient (K_d) values indicated high Cd mobility and strong Pb particle affinity. Structural Equation Modeling (SEM) identified organic matter (OM) and pH as key cross-media regulators. XGBoost-based ecological risk modeling showed robust performance (R^2 = 0.714–0.747), with Cd contamination factor, OM, pH, and K_d as dominant predictors. Zones of high ecological risk were concentrated near the Yalu River estuary. This integrative strategy provides novel tools for tracing pollutant sources, assessing ecosystem health, and guiding transboundary pollution management in the Bohai-Yellow Sea region.

1. Introduction

Heavy metal(loid)s (HMs) are persistent pollutants in coastal environments, with the capacity to accumulate across multiple environmental media and pose long-term ecological risks. In rapidly urbanizing coastal regions of China, heavy metal (HM) contamination is increasingly driven by industrial emissions, agricultural activities, and atmospheric deposition, leading to complex distribution patterns and overlapping pollution sources (Parvin et al., 2025; Wang et al., 2024). Given the high population density and intensive land–sea interactions in these areas, understanding the behavior and risk of HMs has become a critical concern for environmental monitoring and management (Guan

* Corresponding author at: State Key Laboratory of Soil and Sustainable Agriculture, Institute of Soil Science, Chinese Academy of Sciences, Nanjing, 211135, China.
E-mail address: wyhu@issas.ac.cn (W. Hu).

https://doi.org/10.1016/j.marpolbul.2025.118969
Received 21 August 2025; Received in revised form 7 November 2025; Accepted 7 November 2025

et al., 2025).

Previous studies have predominantly focused on HM accumulation and risk assessment within a single medium, such as either soil or sediment (Liang et al., 2019; Liu et al., 2020; Li et al., 2022; Sun et al., 2025). However, this compartmentalized approach overlooks the dynamic interactions among environmental media, particularly in estuaries and their adjacent areas, where surface soil, sediment, and water are functionally coupled via tidal exchange, flooding, erosion, and anthropogenic disturbance (Li et al., 2021). The complexity of such cross-media interactions can obscure the true sources of pollutants and complicate ecological risk predictions. PMF (Positive Matrix Factorization) has been widely applied for source apportionment of environmental media. However, most studies have focused on single medium, such as soil (Fu et al., 2025; Liu et al., 2025), water (Bourtsoukidis et al., 2020; Jahan et al., 2025; Ustaoglu et al., 2025), sediment (Song et al., 2025; Wu et al., 2025a, 2025b), or dust (Han et al., 2025; Khan et al., 2025; Yang et al., 2025a) largely ignoring the interactions and cross-media transport processes that occur in complex environments such as estuaries. In this study, to overcome the limitations of traditional single-medium source apportionment, the PMF model was applied simultaneously to surface soil and sediment samples collected from coastal regions. This integrated multi-media approach enabled a more comprehensive and accurate identification of HM sources.

While PMF provides robust identification of potential pollution sources, it does not account for the quantitative relationships among environmental media or explain how pollutants may transfer or influence each other across media. To further investigate the cross-media interactions and the underlying pathways of HM transport, structural equation modeling (SEM) was employed in this study (Taka et al., 2016; Yang et al., 2025b). SEM enables the construction and testing of causal relationships among observed and latent variables, making it particularly suitable for analyzing how concentrations of heavy metals in one medium may influence levels in another (Chen et al., 2024). By integrating PMF and SEM, this study not only identifies pollution sources but also provides insight into the interconnected behavior of HMs across soil, sediment, and water, which is critical for understanding their fate and for designing targeted pollution control strategies in estuarine and coastal systems. Whereas PMF and SEM provide valuable tools for source identification and causal inference, respectively, both rely on linear assumptions and require careful model specification (Wang et al., 2025a; Wang et al., 2022). These methods may face limitations when dealing with nonlinear relationships, high-dimensional data, and strong multicollinearity among influencing factors—common features in complex environmental systems (He et al., 2022). In recent years, the eXtreme Gradient Boosting (XGBoost) algorithm has gained widespread application in environmental research due to its powerful capabilities in handling nonlinear relationships, high-dimensional datasets, and multicollinearity among variables (Niazkar et al., 2024). For instance, Bhagat et al. (2022) employed XGBoost to predict lead (Pb) concentrations in coastal sediment, effectively identifying key influencing factors such as Copper (Cu), Nickle (Ni), Cerium (Ce), Iron (Fe), average temperature (TEM), and precipitation, thereby improving prediction accuracy and interpretability. Niazkar et al. (2024) further applied XGBoost to assess spatial variations in soil Cu concentrations, where temperature covariates were identified as the dominant drivers. The model demonstrated competitive uncertainty performance compared to advanced spatial models, such as geographically weighted neural networks. Despite these advancements, the application of XGBoost in ecological risk modeling—particularly for indices such as the potential ecological risk index (PERI)—remains limited. Moreover, few studies have explored its potential in multi-media systems such as coastal soil, sediment, and water environments, where complex interactions and cross-media influences prevail. Therefore, this study aims to apply the XGBoost algorithm to predict PERI and analyze the relative importance of influencing factors, providing a novel and data-driven approach for ecological risk assessment in complex coastal systems.

To address the complexity of HM pollution in coastal environments, this study conducted high-density, tri-media sampling (soil, surface sediment, and coastal water) in a typical coastal region of China, and integrated multiple statistical and modeling approaches. Geochemical baselines (GeoBs) were established to assess HM distribution, while PMF and isotope tracing (Cd and Pb) were used for source identification. SEM was applied to quantify cross-media interactions, and XGBoost was employed to predict the PERI and determine the relative importance of key environmental drivers, including physicochemical properties, land use, geography, and meteorology. By combining advanced machine learning with multi-source environmental data, this study proposes a predictive and interpretable strategy for comprehensive ecological risk assessment and management in complex coastal systems.

2. Materials and methods

We consider the coastal areas along the Bohai Sea and Yellow Sea of China as a unified coastal ecosystem, within which surface soil, water,

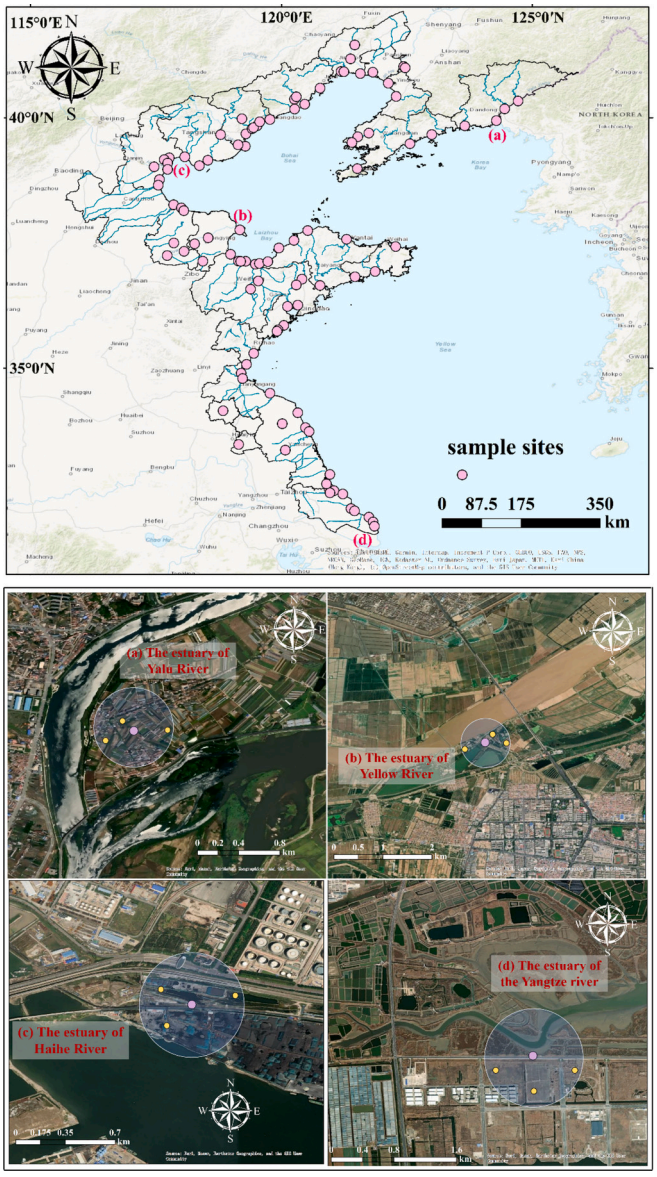

Fig. 1. Sampling sites along the coasts of China and the estuaries of four major rivers. The circular areas in the satellite images indicate a 500 m radius within which soil samples were collected in coordination with nearby sediment and water sampling points.

and sediment were treated as interconnected environmental media (Fig. 1). A total of 103 typical paired soil–sediment–water samples were collected from field investigations conducted in July 2018. The detailed sampling procedures and methodologies can be found in the previously published papers (Liu et al., 2020; Tian et al., 2020). A spatially coupled sampling design was implemented. At each sediment-water site (pink circles, Fig. 1), surface water (0–10 cm) and sediment (0–5 cm) were collected within 5 m. The water and sediment samples were each composited separately to form one representative sample per medium for analysis. For terrestrial linkage, three composite surface soil samples (0–20 cm), each derived from three sub-samples within a 5 × 5 m plot, were collected from distinct locations within a 500 m land buffer centered on each sediment-water site (yellow points, Fig. 1). This provided a robust terrestrial dataset for pairing with each corresponding sediment-water site. Regional-scale sampling in 2018 revealed anomalous Cd and Pb concentrations and partition coefficients (K_d) in soil, sediment, and water of the Yangtze River Delta. Considering the preservation of isotopic signals in soil and sediment (Briant et al., 2024), Cd and Pb isotope samples were subsequently collected between 2021 and 2023 across Jiangsu, Zhejiang, and Shanghai (Tian et al., 2024). This two-stage sampling strategy represents an established approach in environmental geochemical source tracing (Amideina et al., 2025; Araújo et al., 2019; Wu et al., 2025a, 2025b). The detailed sampling procedures and isotope analysis protocols (the calculation of Cd and Pb source contribution rates in soil using both the end-member and Bayesian models) are provided in Text S1.

2.1. Approaches for establishing geochemical baselines

To establish geochemical baselines (GeoBs) for HMs in coastal soil and sediment, we adopted four widely applied statistical approaches: the iterative mean (IMEA) method, iterative median (IMED) method, relative cumulative frequency (RCF) method, and the boxplot method (Carrillo et al., 2022; Sun et al., 2023; Guo et al., 2025). These methods were chosen because they are commonly recommended for environmental geochemistry and provide complementary perspectives for distinguishing natural background from anthropogenic enrichment in heterogeneous coastal settings (Table S6). The four methods were compared to identify the most appropriate approach for this study. To further elucidate the distribution characteristics of HM contamination, a bivariate point-plotting analysis was conducted using soil concentrations on the x-axis and sediment concentrations on the y-axis (Fig. S4). Each plot was divided into four distinct zones: the Background zone represents concentrations below the minimum GeoBs determined by the four statistical methods. The Soil-dominated and Sediment-dominated zones correspond to cases where concentrations fall between the lowest geochemical baseline (GeoB) of one medium and the highest GeoB of the other. The Pollution zone indicates the bivariate domain where both soil and sediment concentrations simultaneously exceed their respective maximum GeoB values, representing dual-media pollution.

2.2. Calculation of the distribution coefficient in sediment-water system

The partitioning behavior of HMs between the aqueous phase and the solid phase in sediment–water systems was evaluated by calculating the distribution coefficient (K_d), which reflects the affinity of HMs for sediment relative to water (Wang et al., 2025b). This parameter is crucial for understanding the mobility, bioavailability, and potential environmental risk of HMs in aquatic environments.

The distribution coefficient (K_d) was calculated using the following equation:

$$K_d = (C_s/C_w) \times 100 \quad (1)$$

Where, $C_s$and C_w are the HM contents in the sediment (mg/kg) and their corresponding contents (μg/L) in the water body. A higher K_d value indicates a greater tendency of the metal to associate with the sediment, implying lower mobility in the aquatic environment.

2.3. Structural equation model (SEM)

Structural equation modeling (SEM) was employed to explore the interactions and transfer pathways of HMs among three environmental media: sediment, soil, and water. The model construction was based on prior geochemical understanding of element mobility and potential environmental exchange processes (Rubab et al., 2025). Latent variables (soil, sediment and water geochemical system) represent sediment, soil, and water were constructed using selected HMs and key physicochemical properties. Specifically, a priori model was first constructed based on the theoretical framework (Fig. S4) and iteratively refined until stability was achieved by removing weakly loaded paths. Latent variables were initially built from a wide set of HMs (Cd, Pb, Cu, Zn, Cr, Ni, Hg, As) and physicochemical properties. To prevent overfitting and improve model accuracy, representative variables were retained, including Cd, Pb, Ni, OM, and pH for sediment and soil, and Cd, Pb, Ni, DO, and pH for water. The model was implemented in R (lavaan package) with standardized inputs, and model fit was evaluated using CFI, TLI, RMSEA, and SRMR (Text S2, Table S3).

2.4. Source apportionment of heavy metals using PMF

To apportion the sources of HMs in the coastal soil–sediment system, the U.S. EPA's Positive Matrix Factorization (PMF 5.0) model was employed (Wu et al., 2025a, 2025b). A total of 103 matched sampling sites were analyzed for 8 HMs (Arsenic (As), Cd, Chromium (Cr), Cu, Mercury (Hg), Ni, Pb, Zinc (Zn)) in soil and sediment, and 7 metals (excluding Hg) in coastal surface water. This yielded datasets of 824 (soil and sediment, respectively) and 721 (water) concentration values for model input. Prior to modeling, the data were pre-processed in accordance with EPA guidelines.

Each medium was modeled separately using 150 bootstrap runs. Four factors were selected based on the minimum Q(Robust), stability of the bootstrap mapping, and interpretability of the factor profiles. Bootstrap results indicated stable factors mapping across 100 % of runs (150/150), confirming the robustness of the four-source solution. Diagnostic evaluation showed good reconstruction performance across most metals, with regression r^2 values ranging from 0.75 (Pb) to 0.92 (Cr). All species passed the KS normality test ($p > 0.05$), indicating no systematic bias in the residuals. The detailed base run parameters for PMF are provided in Supplementary Text S3.

2.5. Potential ecological risk modeling using XGBoost algorithm

To identify key environmental drivers of HM–induced potential ecological risk in the coastal soil–sediment system, we employed a machine learning approach based on the extreme gradient boosting (XGBoost) algorithm (Text S4). The potential ecological risk index (PERI) was calculated for both soil and surface sediment samples using the method by Håkanson (1980), incorporating contamination factors (CF) for eight target HMs. PERI values served as the response variable for model training. A total of 22 predictor variables encompassing geochemical, physicochemical, climatic, anthropogenic, and geological factors were considered. These included pollution and migration indicators, such as the contamination factor (CF) for soil and the sediment–water partition coefficient (K_d) for sediment; Physicochemical properties, including soil/sediment organic matter (OM), pH, dissolved oxygen (DO), and salinity; Geographical and natural attributes, such as digital elevation model (DEM), lithology, and vegetation cover (NDVI); Anthropogenic activity indicators, including population density (POP), enterprise (factory) density, gross domestic product (GDP), and land use type; Meteorological variables, including annual precipitation and

average temperature (TEM).

All predictor variables were standardized prior to modeling. To avoid multicollinearity, retain only the most informative variables within correlated clusters. For feature selection, we initially trained XGBoost model to rank variables based on important scores. The top 10 predictors identified by XGBoost were subsequently used to build the final regression models for PERI in soil and sediment, respectively. To reduce dimensionality and avoid overfitting, we retained only predictors with XGBoost importance scores greater than 0.01. This threshold corresponded to the 10 most informative variables, which together accounted for over 90 % of the total model importance. Additional predictors with lower importance did not improve model performance but increased complexity, and were therefore excluded. Model performance was evaluated using five-fold cross-validation, with coefficient of determination (R^2) and root mean square error (RMSE) as primary metrics. Additionally, SHAP (SHapley Additive exPlanations) values were employed to interpret the contribution and directionality of individual features on PERI outcomes. The final XGBoost model demonstrated robust predictive performance, with R^2 values of 0.714 (soil) and 0.747 (sediment).

3. Results and discussion

3.1. Establishment and comparison of region-specific geochemical baseline values of heavy metals for soil and sediment

We regarded the soil-sediment-water continuum along the coasts of the Yellow Sea and Bohai Sea of China as an integrated environmental system and established region-specific geochemical baseline values to better characterize natural background levels and assess anthropogenic enrichment of HMs. These values were compared with regional background values derived from literature sources. In soil, the GeoBs for Cu, Zn, Cr, Ni, Hg, and As show marked variability. For Cu, Zn, and Cr, the relative cumulative frequency (RCF) method consistently yielded the highest baseline estimates (21.51, 73.59, and 58.13 mg/kg, respectively). In contrast, the iterative mean (IMEA) and median (IMED) methods generally produced lower values for these metals, in some cases significantly below background concentrations, as indicated by bold italics (e.g., Cu: 17.20 mg/kg vs. background 23.34 mg/kg). Hg showed the greatest deviation, with iterative values (0.022–0.023 mg/kg) lower than the background (0.094 mg/kg), while RCF increased it to 0.034 mg/kg. In sediment, a similar pattern emerged, with the RCF method producing the highest values for most HMs. For example, Zn reached 78.26 mg/kg (compared to a background of 56.65 mg/kg), while Pb attained 26.11 mg/kg (compared to a background of 12.72 mg/kg), representing a more than twofold increase. Iterative methods and boxplot analysis generally yielded lower values, and in several cases (Cu, Ni, Hg) produced estimates substantially below regional background levels. Hg again showed pronounced differences, ranging from 0.022 mg/kg (IMED) to 0.058 mg/kg (RCF), compared to a background of 0.023 mg/kg.

Among the four statistical methods tested, the boxplot method was identified as the most suitable approach for establishing the GeoB in this study. This is attributed to its ability to yield consistent and robust results in both soil and sediment matrices. In contrast, the RCF method tends to overestimate the GeoBs, whereas the iterative method shows a tendency to underestimate. The boxplot method, however, consistently produces values that fall within the range bounded by the highest and lowest estimates, thereby offering a more balanced and reliable representation. Notably, Cd and Pb exceeded their background levels under all methods. These findings highlight that methodological differences can substantially influence GeoB estimates, and that for heterogeneous coastal regions, a robust baseline determination should integrate multi-method comparison with source apportionment, taking into account both geological background and anthropogenic contributions (Kuang et al., 2023; Mostafa et al., 2023).

To further elucidate the distribution characteristics of HM contamination, a bivariate scatter plot analysis was conducted with soil concentrations on the x-axis and sediment concentrations on the y-axis (Fig. S4). Additionally, the proportions of sampling sites within each defined zone were statistically evaluated. As shown in Fig. 2, Zn accounts for 33 % in the dual-media pollution zone, while the other 7 HMs range from 22 % to 29 %. Pb reaches 37 % in the dual-media background zone, compared with 20–29 % for the other HMs. Cd shows the highest proportion in the sediment-dominated zone (31 %), whereas Pb is the lowest (11 %), with other HMs ranging from 19 % to 28 %. In the soil-dominated zone, Cd and Zn show lower proportions, while the other HMs are comparable (22–28 %). These results indicate that, except for Cd and Pb, the proportions of other HMs are relatively consistent under the soil–sediment dual-media baseline evaluation system, suggesting similar sources and geochemical behaviors (Wang et al., 2025b). Notably, Cd and Pb exhibit the highest proportions of samples in the Background Zone; however, since these GeoBs exceed the regional natural background values, their presence in this zone does not necessarily indicate the absence of anthropogenic input. Therefore, further investigation into the sources of HMs in the coastal soil–sediment–water system, particularly the natural and anthropogenic inputs of Cd and Pb as well as their transformation factors, is warranted.

3.2. Integrated source identification and spatial characterization of heavy metals in coastal environments

While the establishment of media-specific GeoBs values provided a foundational baseline for assessing enrichment patterns, it does not directly elucidate the pathways or origins of contamination. Therefore, to decipher the source composition and quantify the relative contributions of natural versus anthropogenic inputs across different environmental media, PMF was used to HM datasets from coastal soil and

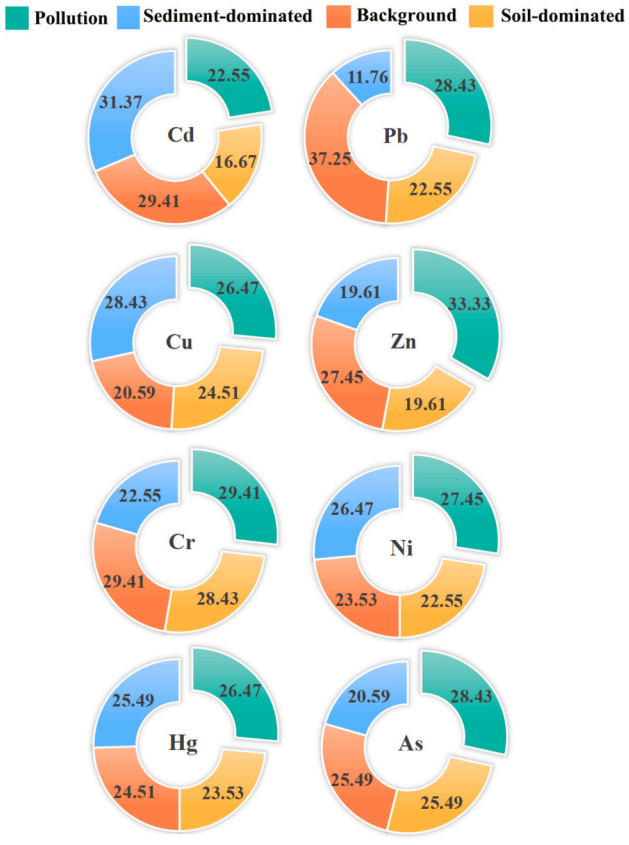

Fig. 2. Partitioning of dominant pollution media and background levels of heavy metals under soil–sediment dual-media geochemical baselines.

sediment (Fig. 3). Four common source factors were identified in all media, albeit with varying contribution rates and metal associations. In coastal soil, Factor 3 (represented by Cu, Zn, Cr, and Ni) contributed the most to total HM concentrations (50.91 %) and was identified as a mixed natural-agricultural source. This grouping aligns well with the observed variability in their GeoBs across different statistical methods (Table 1). The notable difference in GeoB estimates for Cu, Zn, Cr, and Ni reflects their complex distribution patterns in soil, which are likely attributable to overlapping contributions from natural background levels and anthropogenic agricultural activities. GeoBs variability and PMF stability reveal sensitivity to source complexity and underscore the complementary roles of baseline estimation and source apportionment in identifying mixed sources. Cr and Ni are typical weathering products of mafic rock, and their accumulation in coastal soil is primarily controlled by the composition of the parent material (Sahoo et al., 2025). The accumulation of Cu, Zn, and Cr in downstream sediment is influenced by upstream agricultural activities, including the use of pesticides, fertilizers, and biomass inputs (Zhuang et al., 2019). This lithogenic origin is further supported by the much lower GeoBs of soil Cr and Ni compared with their regional background levels (Table 1). Previous studies based on isotopic compositions have shown that industrial activities and atmospheric deposition are the main sources of Cd and Pb inputs to soil and sediment (Bouziane et al., 2025; Xu et al., 2025). In this study, the $^{206}Pb/^{207}Pb$ ratios in surface soils (1.17 ± 0.013 ‰) closely overlap with isotopic signatures of factory (1.166 ‰) and vehicular emissions (1.156 ‰), which directly correspond to Factor 4 in soil (20.41 %) identified as industrial and atmospheric sources (Table S2). This provides a quantitative isotopic constraint that reinforces the PMF attribution to fossil fuel–related activities. Therefore, Factor 4 (20.41 %) in soil can be

Table 1
Comparison of geochemical baseline values for selected HMs in soil and sediment using different statistical approaches.

Trace Elements mg/kg	Iterative mean method (IMEA)	Iterative median method (IMED)	Relative cumulative frequency (RCF)	Boxplot	Background values
Soil					
Cd	0.108	0.100	0.154	0.110	0.100
Pb	23.29	23.30	25.28	23.30	23.18
Cu	***18.00***	***17.20***	***21.51***	***18.70***	23.34
Zn	***58.32***	***58.75***	73.59	***63.40***	69.46
Cr	***55.02***	***57.20***	***58.13***	***56.80***	70.84
Ni	***23.08***	***22.90***	***24.62***	***22.95***	28.44
Hg	***0.023***	***0.022***	***0.034***	***0.025***	0.094
As	***5.87***	***5.90***	***7.44***	***6.52***	10.26
Sediment					
Cd	0.109	0.110	0.171	0.110	0.120
Pb	21.16	20.20	26.11	21.80	12.72
Cu	*17.86*	*17.10*	22.50	18.50	16.59
Zn	61.75	*57.70*	78.26	66.60	56.65
Cr	56.08	53.60	57.33	55.60	52.60
Ni	***23.17***	***22.45***	***23.75***	***22.80***	28.85
Hg	0.023	***0.022***	0.058	0.026	0.023
As	***6.42***	***5.67***	8.854	***7.26***	7.70

Note: Values in bold italics indicate concentrations lower than the corresponding regional background values. Background values are derived from the background value statistics in the relevant regional literature (Table S7).

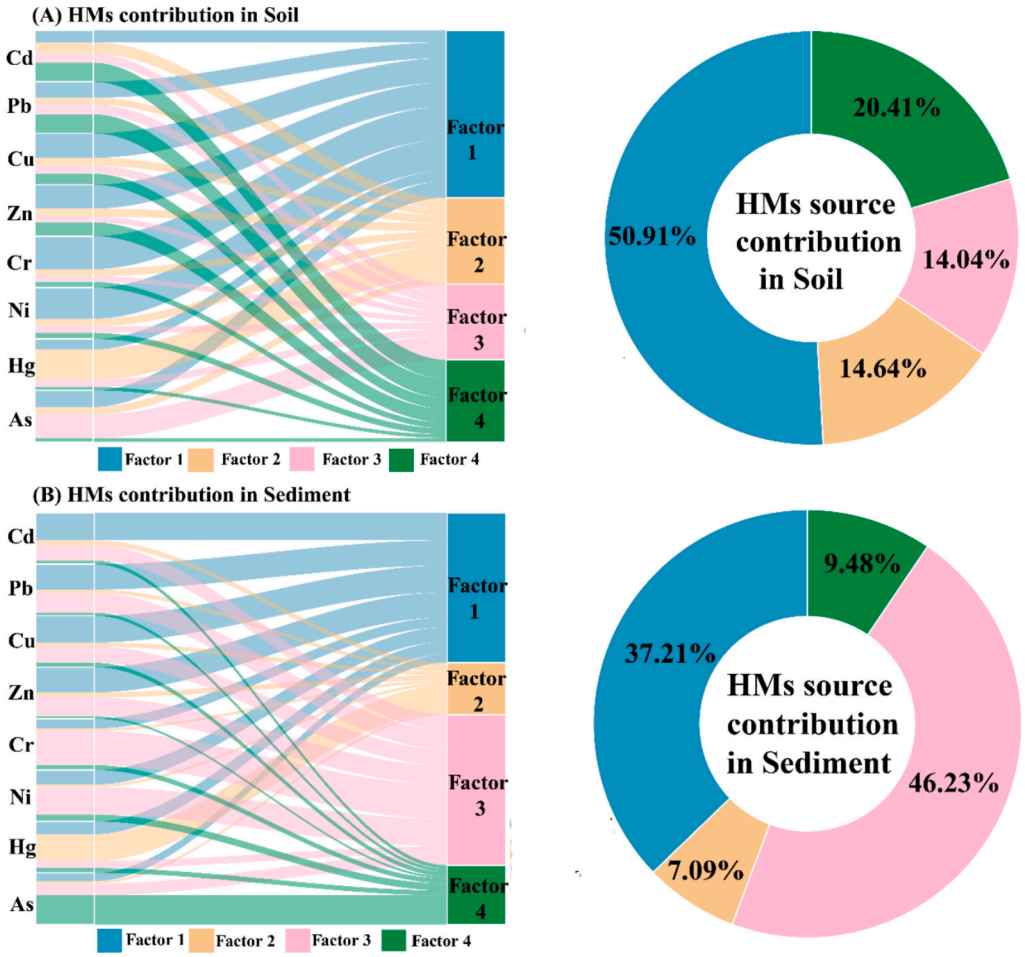

Fig. 3. Source apportionment of HMs in soil and sediment using PMF analysis.

attributed to industrial emissions and atmospheric deposition, likely associated with ship fuel combustion, smelting activities, and long-range atmospheric transport.

In surface sediment, the separation between natural and anthropogenic sources was more distinct. Cr and Ni exhibited the highest loadings in Factor 3 (46.23 %), consistent with their lithogenic origin (Wang et al., 2024b), as these metals are strongly retained in mineral lattices and less mobile in sediment unless under extreme redox conditions (Li et al., 2014). In contrast, Factor 1 (37.21 %), dominated by Cd, Pb, Cu, and Zn, represents a clear anthropogenic input, likely from urban runoff, industrial discharge, and maritime activities, which are known to significantly influence estuarine sediment quality (Ikhsani et al., 2025). Overall, Factor 3 and Factor 1 in sediment represent geogenic (natural geological) and multiple anthropogenic sources, respectively. In this study, PMF analysis consistently separated Hg (soil Factor 2 and sediment Factor 3) and As (soil Factor 3 and sediment Factor 4) into independent factors, suggesting that their sources differ from those of other HMs (e.g., Cd, Pb, Cu, Zn). This interpretation is supported by their distinct biogeochemical behavior, as Hg is volatile and prone to methylation, while As is highly redox-sensitive and often associated with Fe oxides (Cao et al., 2023; Guédron et al., 2024). Furthermore, As showed a significant positive correlation with OM in both soil ($p < 0.01$) and sediment ($p < 0.05$) (Figs. S9 and S10), implying a potential link to OM inputs from agricultural irrigation and runoff. These findings align with previous reports that Hg in estuarine and coastal sediments are largely derived from atmospheric deposition, watershed erosion, and legacy contamination (Yin et al., 2013; Feng et al., 2010; Janssen et al., 2025a, 2025b). Similarly, As mobilization has been attributed to reductive dissolution of Fe/Mn oxides and dissolved organic matter-enhanced microbial processes under irrigation, which transport As via groundwater and surface runoff to estuaries (Xiao et al., 2018; Zhao et al., 2020). Together, these mechanisms help explain the unique factor profiles of Hg and As in our PMF results. The distinct sources and biogeochemical behaviors of Hg and As necessitate tailored control strategies: mitigating Hg requires curtailing atmospheric emissions and managing methylation potential in sediments, whereas controlling As depends on regulating agricultural runoff and preventing its remobilization under reducing conditions.

To further validate and complement the source apportionment results derived from PMF, we integrated sediment-water partitioning behavior and isotopic composition (Cd and Pb) analyses. Fig. 4 illustrates the partition coefficients ($\log_{10}K_d$) of 6 HMs (Cd, Pb, Cu, Zn, Cr, and Ni) across 4 major Chinese river estuaries—Haihe, Yalu, Yangtze, and Yellow Rivers—highlighting spatial differences in metal sediment affinity. Cd exhibited the lowest K_d in the Yangtze estuary, implying weaker sediment association and greater mobility, potentially influenced by elevated dissolved oxygen (DO) levels, salinity gradients, or competitive complexation with other ions (Argun, 2025; Zhang et al., 2025). Although DO shows no significant differences among the 4 river estuaries, the Yangtze estuary had the highest salinity and the Yalu River estuary the lowest. Correspondingly, the highest K_d was observed in the Yalu River estuary (Fig. S10). Spearman correlation (Fig. S14 and Table S9) revealed a significant negative relationship between K_d of Cd and salinity ($\rho = -0.37$, $p < 0.05$), and multiple regression further confirmed salinity as a dominant predictor ($\beta = -0.95$, $p = 0.021$). This indicates that higher salinity promotes Cd mobilization into the dissolved phase through chloro-complexation and competitive ion exchange, thereby lowering K_d of Cd. In comparison, DO exhibited a weak effect on Cd partitioning, but influenced K_d of HMs indirectly through its regulation of water pH, which was positively correlated with K_d of Cd ($\rho = 0.29$, $p < 0.05$). These results highlight that salinity is the primary factor controlling Cd mobility in the estuarine system, while DO acts as a secondary regulator through pH (Lee et al., 2025; Lu et al., 2025). Pb showed the highest K_d in the Yangtze estuary, suggesting enhanced binding to sediment particles, which may be attributed to elevated particulate organic matter, fine-grained sediment, or inputs from upstream anthropogenic sources (Santucci et al., 2024). Zn exhibited moderate-to-high K_d values across estuaries, whereas Cu displayed the lowest sediment affinity in the Haihe estuary and the highest in the Yangtze River, likely due to differences in organic matter complexation and redox conditions. The high $\log_{10}K_d$ values of Cr and Ni in the Yangtze River estuary stem from a combination of source and estuarine

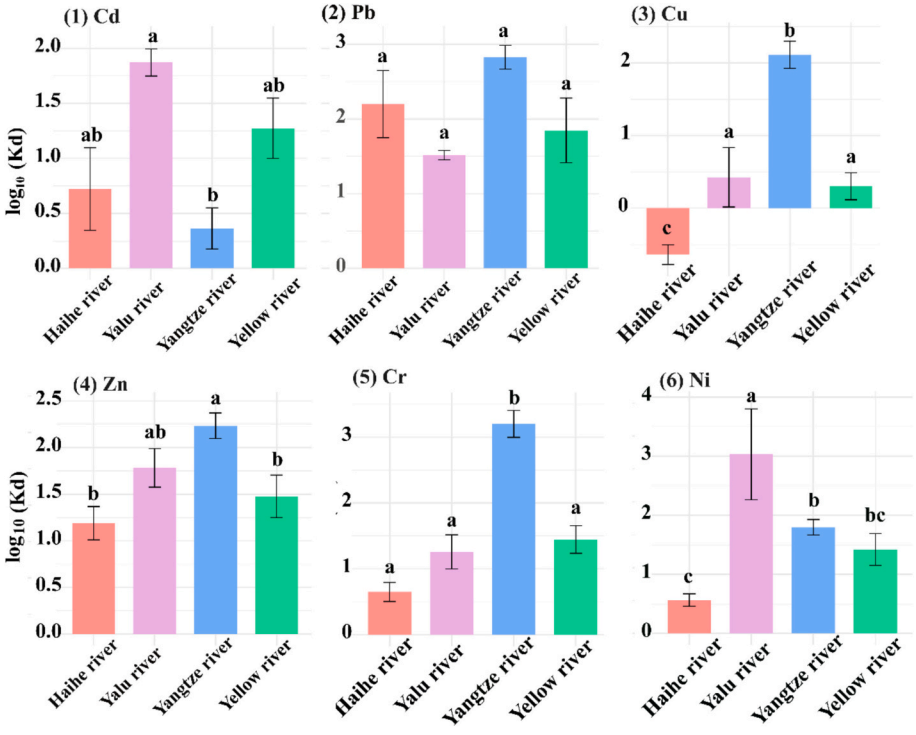

Fig. 4. Comparative analysis of sediment-water partition coefficients (K_d) for Cd, Pb, Cu, Zn, Cr, and Ni in Haihe, Yellow, Yalu, and Yangtze Rivers. (For interpretation of the references to colour in this figure legend, the reader is referred to the web version of this article.)

processes. Their lithogenic origin, confirmed by characteristic Cr/Ni (2.29), Cr/Co (5.84), and Ni/Co (2.60) ratios and strong sediment correlations ($\rho > 0.6$) (Fig. S6), ensures a primary supply of particle-reactive elements (Liou et al., 2000). In addition, the nearly identical background concentrations of Ni in soil (22.95 mg/kg) and sediment (22.80 mg/kg), together with similar Cr patterns (Yan et al., 2021), indicate lithogenic inheritance and parent material control rather than anthropogenic influence. Furthermore, the vertical uniformity of Cr and Ni across 0–100 cm soil profiles (Fig. S17) and their high K_d values demonstrate geochemical stability associated with lattice fixation and solid-phase adsorption (Li et al., 2014a). The high K_d values of Cr and Ni in coastal soil arise from the combined effects of sediment-derived parent material inheritance and mineral lattice fixation, reflecting their strong geochemical stability.

To investigate the relatively high GeoBs of Pb and Cd in sediment and soil, we conducted a high-density sampling campaign in the Yangtze River estuary and analyzed Cd and Pb isotopic compositions. The Pb isotopic composition of deep soil closely resembles that of the Yellow River and Yangtze River sediment, suggesting it primarily derives from background (Cheng et al., 2019; Zhang and Luo, 2011). In contrast, the Pb isotopic signatures of surface soil indicate contributions from anthropogenic sources, including vehicular emissions, coal combustion, and urban activities. By applying a Bayesian two-endmember model jointly constrained by $^{206}Pb/^{207}Pb$ and $^{208}Pb/^{206}Pb$ ratios (Table 2), we estimated that 67 % of Pb originates from parent material and 33 % from atmospheric/industrial sources, which corresponds closely to PMF Factor 4 in soil and Factor 1 in sediment. These samples showed lower $^{206}Pb/^{207}Pb$ and higher $^{208}Pb/^{206}Pb$ ratios, consistent with Pb derived from high-temperature industrial processes and fossil fuel use (Table S2). The Pb isotopic signatures of sediment along the Yangtze River in this study overlap with those of the Yellow River natural sediment and suspended matter, supporting the hypothesis of Yellow River-derived material contribution to the Yangtze River system, consistent with previous evidence of mixed provenance and sediment transport processes in the East China Sea inner shelf mud regions (Zhao et al., 2018). Additionally, some sediment and soil samples exhibit isotopic compositions that overlap with those of atmospheric deposition and traffic-related emissions, indicating anthropogenic influences (Zhou et al., 2024a). Importantly, the Pb isotopic variations correspond closely with PMF-resolved source factors: lighter $^{206}Pb/^{207}Pb$ and higher $^{208}Pb/^{206}Pb$ ratios are characteristic of industrial and atmospheric inputs (PMF Factor 1 in sediment and Factor 4 in soil), while heavier isotopic compositions reflect lithogenic contributions (Factors 2–3). This alignment demonstrates that Pb isotopes effectively trace the same anthropogenic emission sources identified statistically by PMF, particularly those linked to coal combustion, smelting, and vehicular exhaust. The isotopic fractionation arises from high-temperature volatilization and condensation during these industrial processes, which preferentially release radiogenic ^{206}Pb-depleted aerosols, thereby explaining the isotopic signatures detected in both soil and sediment. Thus, Pb isotopes not only validate but also mechanistically support the PMF-identified industrial and atmospheric factors. In this study (Fig. 5b and Table S1), sediment display more negative $\delta^{114}/^{110}Cd$ values than soil ($\Delta^{114/110}Cd_{\text{Sediment-surface soil}} = -0.08$ ‰), This isotopic pattern likely reflects the preferential incorporation of light Cd isotopes into solid phases through adsorption and co-precipitation, combined with enhanced contributions from industrial and atmospheric sources that are isotopically lighter. Repeated water–particle interactions during sediment deposition further promote the retention of lighter Cd isotopes, amplifying the isotopic difference between sediment and soil (Zhong et al., 2021; Zhou et al., 2024b). Surface water was enriched in heavy isotopes ($\Delta^{114/110}Cd_{\text{Surface soil-water}} = -0.18$ ‰), suggesting preferential retention of lighter isotopes in the solid phase and supporting the interpretation that Cd is actively partitioned during transport and adsorption processes (Ip et al., 2004; S. Zhang et al., 2024). Surface soils are enriched in heavy Cd isotopes ($\Delta^{114/110}Cd_{\text{Surface soil-deep soil}} = 0.11$ ‰), whereas deep soils are enriched in light isotopes, mainly due to root uptake, leaching, and differences in organic/oxide binding (Gao et al., 2022). The mean Cd isotopic composition of rice grains was 0.26 ± 0.19 ‰, with heavy isotope enrichment reflecting phloem transport, where light isotopes are retained in stems and leaves via peptide and thiol chelation, and heavier isotopes preferentially translocated to grains (Imseng et al., 2019).

Although direct industrial Cd end-member data were unavailable, the isotopic mixing model suggests that non-natural inputs (atmospheric deposition and fertilizer sources) contribute up to 56 % of Cd in surface soils, consistent with the anthropogenic components identified by PMF (Factor 4 in soil; Factor 1 in sediment). Importantly, the coupling of lighter Cd isotopic signatures with PMF-derived anthropogenic factors reveals underlying geochemical mechanisms: high-temperature industrial and combustion processes preferentially emit isotopically light Cd, while subsequent adsorption and co-precipitation processes in sediments further enhance light isotope retention. Therefore, the Cd isotope fractionation observed in this study provides mechanistic support for the PMF results, confirming that anthropogenic emissions are the dominant source of isotopically lighter Cd in the studied coastal system.

The integration of PMF source apportionment with Cd and Pb isotopic analysis and sediment–water partitioning (K_d) mapping provides a multi-proxy approach for identifying HM sources in coastal environments. The isotopic apportionment for surface soil Pb (approximately 67 % parent; 33 % anthropogenic sources) and Cd (44 % parent; 56 % anthropogenic sources) quantitatively strengthen the linkage between isotopic evidence and PMF-resolved factors. Pb and Cd isotopic signatures together provide direct geochemical evidence of anthropogenic contributions, aligning with PMF factors dominated by industrial emissions, atmospheric deposition, and urban runoff. In contrast, Cr and Ni exhibited geochemical behaviors indicative of strong geochemical stability, as reflected by their high K_d values, strong retention in sediment, and weak enrichment relative to GeoBs. The consistency among PMF modeling, K_d patterns, and isotopic tracers (for Cd and Pb) highlights the value of combining geochemical and statistical tools for source differentiation.

Table 2
Source contribution of Pb and Cd in surface soils based on isotope mixing models.

Isotope and model	Weathering of parent material %				Atmospheric deposition %	
	Range		Mean		Range	Mean
$^{206}Pb/^{207}Pb$ [a]	/		67.8		/	32.2
$^{208}Pb/^{206}Pb$ [a]			67.0			33.0
Bayesian model	55–79		67		21–45	33
Isotope $^{114/110}Cd$	Weathering of parent material %		Atmospheric deposition %		Compound fertilizer %	
	Range	Mean	Range	Mean	Range	Mean
Bayesian model	31–56	44	28–53	42	5–25	14

Note: a' denotes values calculated using the two-endmember model.

3.3. Path coefficient diagram of influencing factors of heavy metals by SEM

PMF and isotope analyses identified HM sources, while SEM revealed their cross-media interactions in the coastal soil–sediment–water system (Fig. 6). Additionally, the covariance between the sediment and water phases reflects the bidirectional exchange of HMs across their geochemical systems. This link, showing a marginally significant direct effect ($\beta = 0.19$, $p = 0.099$), may reflect pulse-driven or episodic exchanges facilitated by tidal pumping, storm surges, or bottom shear stress (Chen et al., 2022). Such mechanisms are known to transiently resuspend and redistribute sediment-bound metals into the overlying water column, particularly in estuarine environments (Miranda et al., 2021).

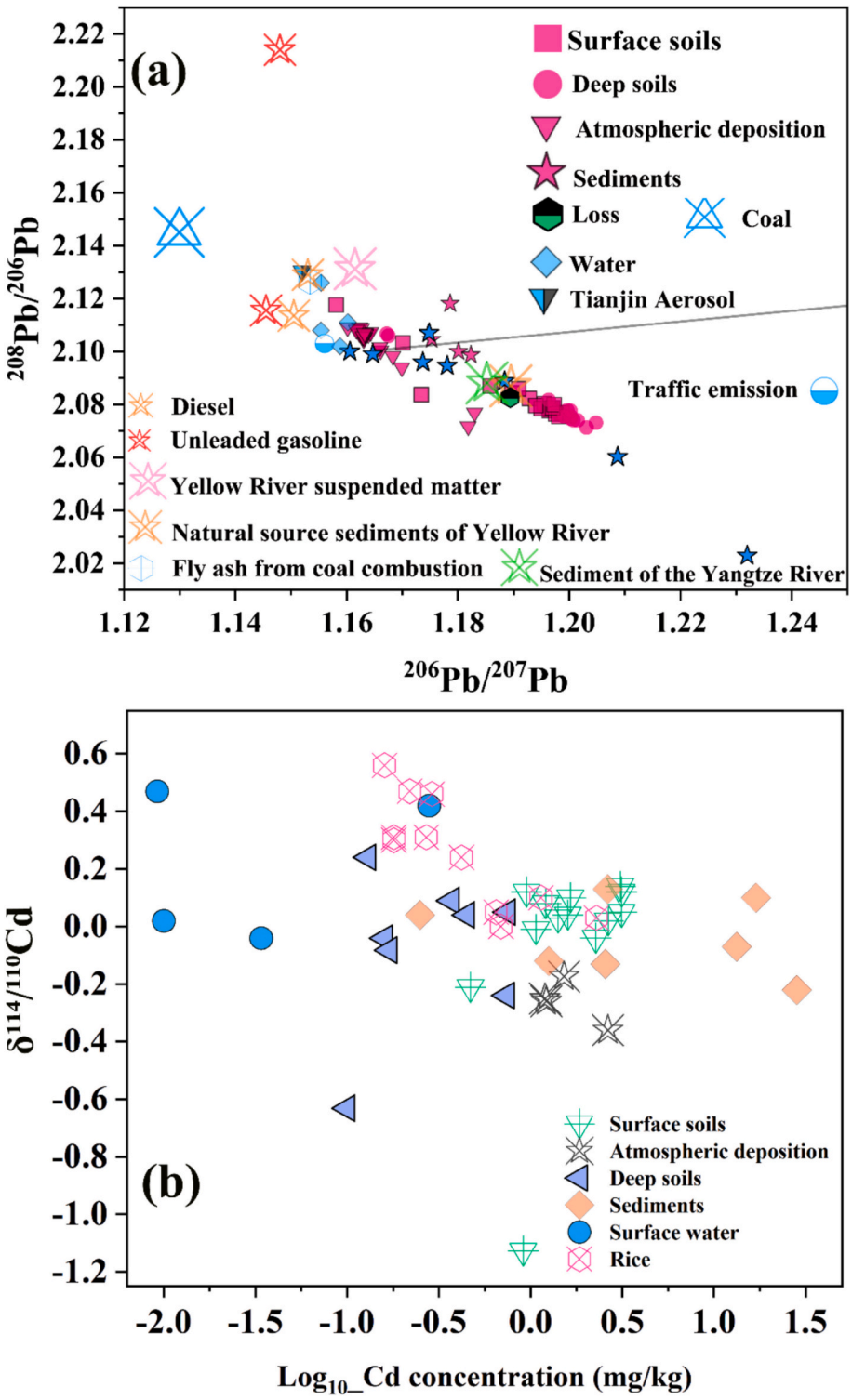

Fig. 5. Pb and Cd isotopic compositions and their implications for source identification in the Yangtze River delta. (a): The red square, circle, triangle, and star symbols represent data from this study, while the others indicate literature-based comparison data. (a) and (b) from the Text S1. (For interpretation of the references to colour in this figure legend, the reader is referred to the web version of this article.)

Within individual geochemical systems, physicochemical factors showed consistent regulatory effects. OM exhibited strong positive standardized effects on the soil and sediment geochemical systems constructed with HMs and chemical properties, with path coefficients of 0.68 and 0.98, respectively (Salgado et al., 2025; Zhou et al., 2024b). Conversely, pH showed negative path loadings in soil (−0.40) and sediment geochemical systems (−0.39), in line with the enhanced solubility and mobility of metals under acidic conditions (Debnath et al., 2021). In the aquatic geochemical system, pH exerted a significant positive standardized direct effect. In contrast, Cd showed a weak negative association and Ni and Pb displayed negative effects, highlighting that estuarine salinity gradients and redox fluctuations favor the retention of Cd in the dissolved phase while promoting the particulate partitioning of Ni and Pb (Goltnik et al., 2022; Fang et al., 2025). SEM

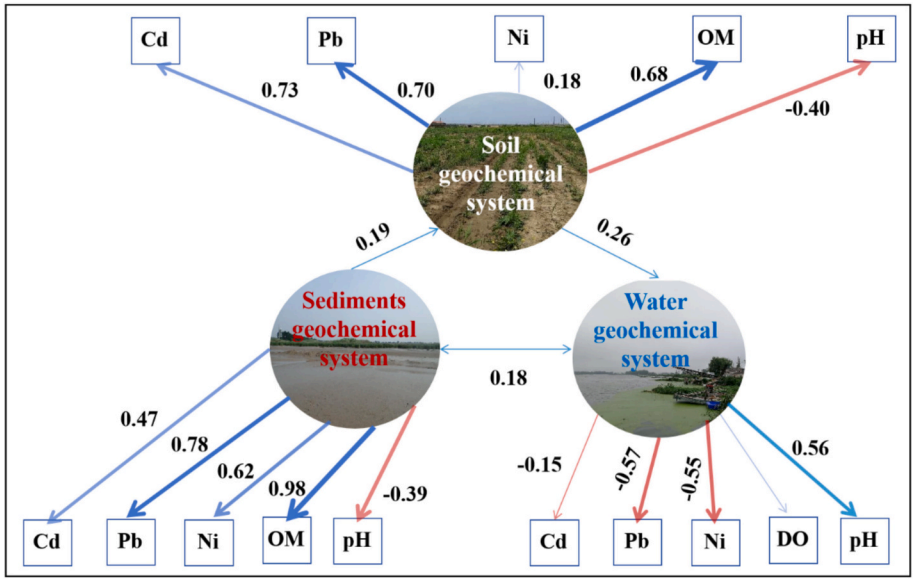

Fig. 6. Structural equation model (SEM) describing the interactions among heavy metals and environmental factors across sediment, soil, and water. Arrows represent standardized path coefficients: blue arrows indicate positive relationships, and red arrows denote negative relationships. The magnitude of each path coefficient is labeled along the arrows. The transparency (opacity) of each arrow reflects the statistical significance of the path: darker arrows indicate stronger significance ($p < 0.05$), while lighter arrows correspond to marginal or nonsignificant paths ($p > 0.05$). (For interpretation of the references to colour in this figure legend, the reader is referred to the web version of this article.)

results revealed that OM enhances HM retention in soil and sediment, while lower pH promotes HM solubility and mobility in soil and sediment but facilitates HM stabilization in water. The marginally significant sediment-water linkage suggests episodic HM exchanges driven by hydrodynamic disturbances. These findings underscore that acidification and OM loss increase HM risks, highlighting the need to control both external inputs and internal cycling across the soil-sediment-water continuum.

3.4. Spatial prediction and machine learning-based interpretation of ecological risk of heavy metals from soil and sediment HMs

SEM revealed HM interactions, and ensemble learning assessed PERI and key ecological risk drivers. The XGBoost model demonstrated strong predictive performance (R^2_soil = 0.714, R^2_sediment = 0.747), validating its suitability for integrating multiple geochemical, climatic, and anthropogenic variables (Fig. 7). Feature importance analysis (Gain and SHAP values) revealed that CF_Cd (contamination factor of Cd) was the dominant contributor to soil PERI (Fig. 7A and Fig. S12), underscoring the critical role of anthropogenic Cd input—likely derived from agricultural activities, industrial emissions, and atmospheric deposition (Barkhordari and Qi, 2025). Soil OM and pH also emerged as key predictors of soil PERI, consistent with the SEM-derived pathways, which show that OM positively regulates HM retention through complexation, thereby mitigating ecological risk. In contrast, lower pH enhances metal solubility and mobility, increasing potential ecological risk (Li et al., 2024). Notably, acidic soil conditions (low pH) were associated with elevated PERI values, reflecting increased metal solubility and bioavailability, particularly for Cd, Pb, and Zn. In addition to geochemical properties, soil pH and OM are influenced by local temperature, precipitation, and land use patterns, which in turn regulate the bioavailability of HMs and consequently shape ecological risk (Tao et al., 2023; L. Wang et al., 2024). Population density and lithology also contributed to spatial variation in risk. Soil developed over shale or acid plutonic and intermediate volcanic rocks inherently exhibit elevated background levels of Cr and Ni, which may interact synergistically with anthropogenic inputs to exacerbate ecological risks in certain regions (Fig. S7). These results align with the findings from SEM and PMF, suggesting that both intrinsic natural controls and external anthropogenic pressures jointly shape the ecological risk pattern across coastal environments (Wang et al., 2024a). Overall, the integration of SEM and XGBoost frameworks provides a mechanistic-to-predictive continuum,

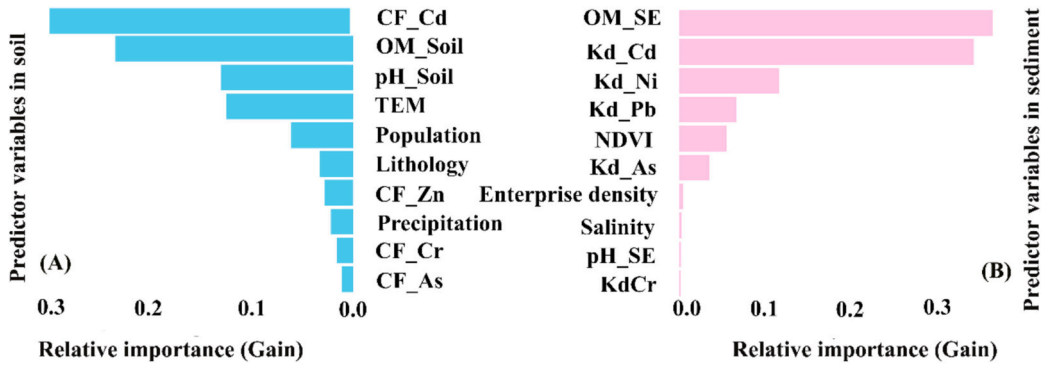

Fig. 7. Prediction of the potential ecological risk (PERI) of HMs in soil and sediment with XGBoost. CF: Contamination factor; OM: Organic matter; K_d: Sediment–water partition coefficient; TEM: Temperature; NDVI: Normalized Difference Vegetation Index.

enhancing our understanding of how HM sources, environmental processes, and landscape features converge to influence ecological outcomes. Such insights are essential for developing media-specific and regionally adaptive management strategies for coastal HM pollution. Unlike the soil model, which was dominated by contamination factors and intrinsic soil properties, the sediment PERI was primarily influenced by sediment organic matter (OM_SE) and metal partitioning behavior, as reflected by distribution coefficients (K_d) of Cd, Ni, and Pb (Fig. 4 and S8). OM_SE ranked highest in both Gain and SHAP analyses, underscoring its critical role in regulating the mobility and fate of HMs in aquatic environments. OM in sediment can either sequester metals through strong binding or facilitate their release under anoxic or acidic conditions (Li et al., 2024). The positive association between OM_SE and predicted PERI suggests that metal-rich organic sediment pose greater ecological risks (Wang et al., 2021a, 2021b), possibly due to long-term accumulation and potential remobilization. K_d represents the equilibrium distribution of metals between solid and aqueous phases. High K_d values for Cd, Ni, and Pb were associated with elevated PERI, suggesting that these metals are not only abundant in sediment but also prone to environmental release under changing redox or salinity conditions (Wang et al., 2023). K_d serves as a mechanistic indicator of metal lability and ecological availability, making it a robust predictor in aquatic risk modeling. Environmental and anthropogenic indicators, such as the normalized difference vegetation index (NDVI) and enterprise density, showed moderate importance (Gong et al., 2023). These variables reflect the influence of land cover, vegetation filtering, and industrial activity on pollutant inputs and hydrological transport. Regions with low vegetation cover or dense industrial presence are more likely to receive and retain metal inputs in sediment bodies (Yang et al., 2022; Zhao et al., 2023). Collectively, the integration of XGBoost modeling with geochemical parameters such as K_d and OM provides a powerful tool to disentangle complex pollutant-sediment interactions and support more effective ecological risk assessment in dynamic coastal systems.

The spatial distribution of the observed and predicted PERI values for soil and sediment revealed a consistent pattern of high-risk areas, predominantly concentrated in the northern coastal region of the study area, particularly at the northeastern tip of the Liaodong Peninsula near the Yalu River estuary (Fig. 8 and S13). The elevated ecological risk at the Yalu River estuary can be attributed to intensive upstream industrial and agricultural activities, coupled with the estuarine sedimentary environment that favors the accumulation and persistence of HMs (Liu et al., 2023a, 2023b). Notably, these areas exhibited the highest PERI values for both media (Soil_PERI_raw = 370.509; Sediment_PERI_raw = 359.323, Table S8), which remained relatively elevated even after model prediction (Soil_PERI_pre = 340.398; Sediment_RERI_pre = 330.957), suggesting persistent ecological pressure in this region. In contrast, the southern coastal regions, including Jiangsu Province, exhibited moderate to low PERI levels, which can be attributed to the significant decline in HM pollution risks as a result of China's effective prevention and control policies, as well as early remediation efforts and natural attenuation processes (Li et al., 2022). Model prediction through XGBoost slightly reduced the extreme PERI values, indicating a smoothing effect that corrects for local variability and highlights broader spatial trends. The strong consistency between observed and predicted distributions also validates the robustness of the predictive model in capturing the spatial heterogeneity of heavy metal–induced ecological risks across coastal zones. Our results demonstrate that integrating XGBoost with geochemical, geographical, and socio-environmental indicators not only provides reliable predictions of current ecological risks, but also offers a promising framework for scenario forecasting under land-use change and anthropogenic pressures. However, given that climate change may substantially alter the physicochemical properties of the nearshore water–sediment–soil system (>Guan et al., 2025), the application of our model to future scenarios remains subject to certain uncertainties. Therefore, future research should incorporate additional climate-related environmental factors and couple machine learning approaches with process-based models of land–sea interactions to enhance the applicability and predictive robustness of the framework under changing climate conditions.

4. Conclusion and limitations

We established region-specific geochemical baselines (GeoBs) for HMs along the Yellow Sea and Bohai Sea coasts of China, with the boxplot method identified as the most suitable approach, and consistently revealed Cd and Pb enrichment above background levels. PMF and pollution zone analyses indicated mixed natural–anthropogenic sources for Cd, Cu, Cr, and Ni in both soil and sediment, with Hg in sediment linked to atmospheric deposition and watershed runoff, and As in soil associated with irrigation and redox mobilization. Pb isotopic compositions distinguished natural sediment-derived Pb from anthropogenic inputs such as traffic emissions and coal combustion. Cd isotopes revealed isotopic fractionation between media, with lighter isotopes preferentially retained in sediment and heavier isotopes enriched in surface waters-patterns consistent with active partitioning and anthropogenic loading identified by PMF. Sediment–water partitioning coefficients (K_d) together with SEM analysis highlighted organic matter (OM) and pH as common cross-media drivers, with salinity and redox conditions exerting stronger control in sediment. Ensemble machine learning (XGBoost) accurately predicted ecological risk, identifying Cd contamination in sediment, as well as OM, pH, and K_d in both soil and sediment, with hotspots concentrated near the Yalu River

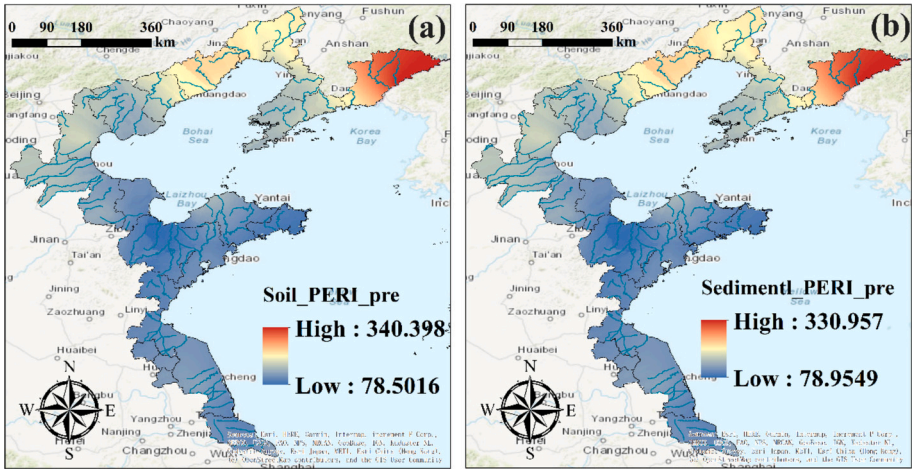

Fig. 8. Spatial distribution of the predicted potential ecological risk index (PERI) for soil (a) and sediment (b) in the coastal region.

estuary. This integrative paradigm enhances mechanistic understanding, source tracing, and predictive capacity for HMs in transboundary coastal systems, offering transferable strategies for pollution control and ecosystem restoration in the Bohai–Yellow Sea and similar regions worldwide.

Although the integration of PMF with Cd and Pb isotopes provides valuable insights into the source apportionment of coastal HMs, future studies should further expand isotopic applications to other elements such as Cr, Ni, Hg, and As. In addition, coupling high-resolution monitoring with process-based experiments across land–marine continua will improve the tracing of HM pathways from upstream to estuaries and better capture seasonal dynamics and interfacial exchanges. These advances will further strengthen the applicability of this integrated framework for sustainable coastal management.

CRediT authorship contribution statement

Qiumei Wu: Writing – review & editing, Writing – original draft, Methodology, Investigation, Formal analysis, Conceptualization. **Peng Liu:** Visualization, Investigation, Data curation. **Shiyi Zhang:** Investigation, Data curation. **Guojing Yan:** Software, Methodology. **Kang Tian:** Validation, Investigation, Conceptualization. **Wenyou Hu:** Supervision, Project administration, Investigation, Funding acquisition. **Tieyu Wang:** Writing – review & editing, Supervision, Project administration. **Jong Seong Khim:** Writing – review & editing, Supervision. **Seongjin Hong:** Writing – review & editing, Supervision, Project administration, Formal analysis. **Bong-Oh Kwon:** Writing – review & editing, Supervision. **Ya''nan Fan:** Validation, Methodology, Formal analysis. **Biao Huang:** Writing – review & editing, Validation, Supervision, Methodology.

Declaration of competing interest

The authors declare that they have no known competing financial interests or personal relationships that could have appeared to influence the work reported in this paper.

Acknowledgments

This study was financed by the National Natural Science Foundation of China (42477438, 41877512), the Agricultural Science and Technology Independent Innovation Foundation of Jiangsu Province China (CX (21)2034). This work was also supported by grant from the National Research Foundation of Korea (RS-2024-00322608).

Appendix A. Supplementary data

Supplementary data to this article can be found online at https://doi.org/10.1016/j.marpolbul.2025.118969.

Data availability

Data will be made available on request.

References

Amideina, A., Orani, A.M., Azemard, S., Gasser, B., Masqué, P., Swarzenski, P., Vassileva, E., 2025. Baseline trace element concentrations in marine sediment from the west African coast. Mar. Pollut. Bull. 215, 117926. https://doi.org/10.1016/j.marpolbul.2025.117926.

Araújo, D.F., Ponzevera, E., Briant, N., Knoery, J., Sireau, T., Mojtahid, M., Brach-Papa, C., 2019. Assessment of the metal contamination evolution in the Loire estuary using cu and Zn stable isotopes and geochemical data in sediments. Mar. Pollut. Bull. 143, 12–23. https://doi.org/10.1016/j.marpolbul.2019.04.034.

Argun, Y.A., 2025. Examination of heavy metal concentrations and their interaction with anthropogenic sources in Ermenek dam Lake (turquoise Lake). Environ. Geochem. Health 47 (2). https://doi.org/10.1007/s10653-025-02367-2.

Barkhordari, M.S., Qi, C., 2025. Prediction of zinc, cadmium, and arsenic in european soils using multi-end machine learning models. J. Hazard. Mater. 490, 137800. https://doi.org/10.1016/j.jhazmat.2025.137800.

Bhagat, S.K., Tiyasha, T., Kumar, A., Malik, T., Jawad, A.H., Khedher, K.M., Yaseen, Z.M., 2022. Integrative artificial intelligence models for Australian coastal sediment lead prediction: an investigation of in-situ measurements and meteorological parameters effects. J. Environ. Manag. 309. https://doi.org/10.1016/j.jenvman.2022.114711.

Bourtsoukidis, E., Pozzer, A., Sattler, T., Matthaios, V.N., Ernle, L., Edtbauer, A., Williams, J., 2020. The Red Sea deep water is a potent source of atmospheric ethane and propane. Nature. Communications 11 (1). https://doi.org/10.1038/s41467-020-14375-0.

Bouziane, M., Terrouche, A., Naidja, L., Ali-Khodja, H., Huang, Z., 2025. Impact of industrial and traffic changes on atmospheric dust and trace element deposition in Didouche Mourad. Algeria. Journal of Hazardous Materials 492. https://doi.org/10.1016/j.jhazmat.2025.138014.

Briant, N., Knoery, J., Araújo, D.F., Ponzevera, E., Chouvelon, T., Bruzac, S., Brach-Papa, C., 2024. Vanishing lead in the Loire River estuary: an example of successful environmental regulation. Environ. Pollut. 340, 122860. https://doi.org/10.1016/j.envpol.2023.122860.

Cao, F., Yang, S., Yin, D., Wang, R., 2023. Geochemical controls on the distribution of total mercury and methylmercury in sediments and porewater from the Yangtze River estuary to the East China Sea. Sci. Total Environ. 892, 164737. https://doi.org/10.1016/j.scitotenv.2023.164737.

Carrillo, K.C., Rodriguez-Romero, A., Tovar-Sanchez, A., Ruiz-Gutierrez, G., Fuente, J.R. V., 2022. Geochemical baseline establishment, contamination level and ecological risk assessment of metals and as in the Limoncocha lagoon sediments, Ecuadorian Amazon region. J. Soils Sediments 22 (1), 293–315. https://doi.org/10.1007/s11368-021-03084-w.

Chen, L., Liu, C., Yin, Y., Liu, G., Li, Y., Cai, Y., 2022. Mass budget of mercury (hg) in the seawater of eastern China marginal seas: importance of the sediment-water transport processes. Environ. Sci. Technol. 56 (16), 11418–11428. https://doi.org/10.1021/acs.est.2c03261.

Chen, X., Wang, Y., Hou, Q., Liao, X., Zheng, X., Dong, W., Zhang, X., 2024. Significant correlations between heavy metals and prokaryotes in the Okinawa trough hydrothermal sediments. J. Hazard. Mater. 479. https://doi.org/10.1016/j.jhazmat.2024.135657.

Cheng, Y., Zhang, R., Li, T., Zhang, F., Russell, J., Guan, M., Wang, X., 2019. Spatial distributions and sources of heavy metals in sediments of the Changjiang estuary and its adjacent coastal areas based on mercury, lead and strontium isotopic compositions. Catena 174, 154–163. https://doi.org/10.1016/j.catena.2018.10.039.

Debnath, A., Singh, P.K., Sharma, Y.C., 2021. Metallic contamination of global river sediments and latest developments for their remediation. J. Environ. Manag. 298. https://doi.org/10.1016/j.jenvman.2021.113378.

Fang, S., Hua, C., Yang, J., Liu, F., Wang, L., Wu, D., Ren, L., 2025. Combined pollution of soil by heavy metals, microplastics, and pesticides: mechanisms and anthropogenic drivers. J. Hazard. Mater. 485, 136812. https://doi.org/10.1016/j.jhazmat.2024.136812.

Feng, X., Foucher, D., Hintelmann, H., Yan, H., He, T., Qiu, G., 2010. Tracing mercury contamination sources in sediments using mercury isotope compositions. Environ. Sci. Technol. 44 (9), 3363–3368. https://doi.org/10.1021/es9039488.

Fu, F., Wang, S., Zhang, X., Xia, Y., Deng, H., Zhao, Y., Ge, C., 2025. Soil-aged microplastics exhibit stronger effects than air- and rainwater-aged ones on the network complexity and assembly process of soil microbial community. Journal of environmental. Chem. Eng. 13 (2). https://doi.org/10.1016/j.jece.2025.115551.

Gao, T., Zhou, J., Zhang, P., Wang, W., Zhou, T., Li, Z., Wu, L., 2022. Cadmium isotope fractionation during transport processes within agricultural soil profiles in a mining area: implications for source tracing. Environ. Pollut. 314, 120327. https://doi.org/10.1016/j.envpol.2022.120327.

Goltnik, T., Burger, J., Kranjc, I., Turšič, J., Zuliani, T., 2022. Potentially toxic elements and Pb isotopes in mine-draining Meža River catchment (NE Slovenia). Water 14 (7), 998. https://doi.org/10.3390/w14070998.

Gong, J., Ouyang, W., He, M., Lin, C., 2023. Heavy metal deposition dynamics under improved vegetation in the middle reach of the Yangtze River. Environ. Int. 171, 107686. https://doi.org/10.1016/j.envint.2022.107686.

Guan, X., Huang, H., Ke, X., Cheng, X., Zhang, H., Chen, A., Wei, C., 2025. Monitoring, modeling, and forecasting long-term changes in coastal seawater quality due to climate change. Nature. Communications 16 (1). https://doi.org/10.1038/s41467-025-57913-4.

Guédron, S., Tolu, J., Amouroux, D., Tessier, E., Molina, C., Bueno, M., Acha, D., 2024. Arsenic, selenium, and mercury speciation in hypersaline lakes of the Andean Altiplano: Link between extreme levels and biodiversity repartition. J. Geochem. Explor. 267, 107577. https://doi.org/10.1016/j.gexplo.2024.107577.

Guo, Y., Zhang, J., Li, H., Liu, Y., Gui, H., Chen, S., Chen, B., 2025. Determination and application of soil heavy metal geochemical baseline in the southern region of Wushan County in the Yangtze River basin, China. Sci. Rep. 15 (1). https://doi.org/10.1038/s41598-025-86404-1.

Håkanson, L., 1980. An ecological risk index for aquatic pollution-control-A sedimentological arrroach. Water Res. 14 (8), 975–1001. https://doi.org/10.1016/0043-1354(80)90143-8.

Han, X., Li, W., Jia, Q., Guo, Z., Zhao, Y., Zhuang, Y., Wu, C., 2025. Multimedia-based source apportionment and health implications of indoor organophosphate esters in various scenes of urban Beijing. China. Environmental Science and Technology 59 (15), 7574–7587. https://doi.org/10.1021/acs.est.4c14450.

He, M., Tang, L., Li, C., Ren, J., Zhang, L., Li, X., 2022. Dynamics of soil organic carbon and nitrogen and their relations to hydrothermal variability in dryland. J. Environ. Manag. 319. https://doi.org/10.1016/j.jenvman.2022.115751.

Ikhsani, I.Y., Harmesa, H., Budiyanto, F., Thoha, H., Fitriya, N., Kaisupy, M.T., Lestari, L., 2025. Heavy metals contamination in Jakarta Bay sediment: geoaccumulation assessment and implication for environmental health. Mar. Pollut. Bull. 216. https://doi.org/10.1016/j.marpolbul.2025.117983.

Imseng, M., Wiggenhauser, M., Keller, A., Mueller, M., Rehkamper, M., Murphy, K., Bigalke, M., 2019. Towards an understanding of the cd isotope fractionation during transfer from the soil to the cereal grain. Environ. Pollut. 244, 834–844. https://doi.org/10.1016/j.envpol.2018.09.149.

Ip, C.C.M., Li, X.D., Zhang, G., Farmer, J.G., Wai, O.W.H., Li, Y.S., 2004. Over one hundred years of trace metal fluxes in the sediments of the Pearl River estuary. South China. Environmental Pollution 132 (1), 157–172. https://doi.org/10.1016/j.envpol.2004.03.028.

Jahan, A., Rai, N., Khan, M.U., 2025. Groundwater contamination characterization and source apportionment of heavy metals and associated source-specific health risk appraisal using Monte Carlo simulation coupled with PCA-MLR and PMF models in the middle Gangetic Basin. India. Exposure and Health 1-32. https://doi.org/10.1007/s12403-025-00693-5.

Janssen, S.E., Hoffman, J.C., Krabbenhoft, D.P., 2025a. New tools for a legacy problem: how isotope tracers inform area of concern actions in the St. Louis river in Lake Superior. J. Great Lakes Res. 51 (1). https://doi.org/10.1016/j.jglr.2024.102494.

Janssen, S.E., Tate, M.T., Dantoin, E.D., Filstrup, C.T., Reavie, E.D., Stewart, R.M., Krabbenhoft, D.P., 2025b. Connecting tributary mercury loads to nearshore and offshore sediments in Lake Superior. J. Great Lakes Res. 51 (1). https://doi.org/10.1016/j.jglr.2024.102381.

Khan, R., Basir, M.S., Anik, A.H., Akhi, S.Z., Khan, M.H.R., Sultana, S., Roy, D.K., 2025. Sources and distribution of potentially toxic elements in urban road dust: A comparative insights and risk assessment of two polluted cities. Environ. Pollut. 368. https://doi.org/10.1016/j.envpol.2025.125768.

Kuang, Z., Wang, H., Han, B., Rao, Y., Gong, H., Zhang, W., Huang, H., 2023. Coastal sediment heavy metal(loid) pollution under multifaceted anthropogenic stress: insights based on geochemical baselines and source-related risks. Chemosphere 339, 139653. https://doi.org/10.1016/j.chemosphere.2023.139653.

Lee, J.W., Jo, A.H., Kang, Y.J., Lee, D., Choi, C.Y., Kang, J.C., Kim, J.H., 2025. Review of cadmium bioaccumulation in fish exposed to cadmium. Toxics 13 (1). https://doi.org/10.3390/toxics13010007.

Li, C., Zhang, Y., Chen, R., Wang, N., Liu, J., Liu, F., 2024. Influence of mineralized organic carbon in marine sediments on ecological heavy metal risk: Bohai Bay case study. Environ. Res. 240, 117542. https://doi.org/10.1016/j.envres.2023.117542.

Li, K., Wang, J., Zhang, Y., 2022. Heavy metal pollution risk of cultivated land from industrial production in China: spatial pattern and its enlightenment. Sci. Total Environ. 828, 154382. https://doi.org/10.1016/j.scitotenv.2022.154382.

Li, M., Zhu, S., Ouyang, T., Tang, J., Tang, Z., 2021. Magnetic properties of the surface sediments in the Yellow River estuary and Laizhou Bay, Bohai Sea, China: implications for monitoring heavy metals. J. Hazard. Mater. 410. https://doi.org/10.1016/j.jhazmat.2020.124579.

Li, Y., Zuo, R., Bai, Y., Yang, M., 2014. The relationships between magnetic susceptibility and elemental variations for mineralized rocks. J. Geochem. Explor. 146, 17–26. https://doi.org/10.1016/j.gexplo.2014.07.010.

Li, Y., Zhang, H., Chen, X., Tu, C., Luo, Y., Christie, P., 2014a. Distribution of heavy metals in soils of the Yellow River Delta: concentrations in different soil horizons and source identification. J. Soils Sediments 14 (6), 1158–1168. https://doi.org/10.1007/s11368-014-0861-0.

Liang, J., Liu, J., Xu, G., Chen, B., 2019. Distribution and transport of heavy metals in surface sediments of the Zhejiang nearshore area, East China Sea: sedimentary environmental effects. Mar. Pollut. Bull. 146, 542–551. https://doi.org/10.1016/j.marpolbul.2019.07.001.

Liou, J., Zhang, R., Jahn, B., 2000. Petrological and geochemical characteristics of ultrahigh-pressure metamorphic rocks from the Dabie-Sulu terrane, east-Central China. Int. Geol. Rev. 42 (4), 328–352. https://doi.org/10.1080/00206810009465086.

Liu, N., Li, X., Chen, P., Yuan, W., Wang, D., Wang, X., 2025. Climate and vegetation controlling accumulation and translocation of heavy metals in water tower regions of Qinghai-Tibet plateau. J. Hazard. Mater. 484, 136752. https://doi.org/10.1016/j.jhazmat.2024.136752.

Liu, P., Hu, W., Tian, K., Huang, B., Zhao, Y., Wang, X., Khim, J.S., 2020. Accumulation and ecological risk of heavy metals in soils along the coastal areas of the Bohai Sea and the Yellow Sea: A comparative study of China and South Korea. Environ. Int. 137. https://doi.org/10.1016/j.envint.2020.105519.

Liu, P., Wu, Q., Hu, W., Tian, K., Huang, B., Zhao, Y., 2023b. Comparison of heavy metals in riverine and estuarine sediments in the lower Yangtze River: distribution, sources, and ecological risks. Environ. Technol. Innov. 30, 103076. https://doi.org/10.1016/j.eti.2023.103076.

Liu, Y., Cheng, Y., Du, Y., Li, H., Li, F., Sun, Y., 2023a. Sedimentary records of heavy metals in the middle reaches of the Yalu River since 1939. Transactions of Oceanology and Limnology 45 (2), 55–63. https://doi.org/10.13984/j.cnki.cn37-1141.2023.02.007. (Chinese).

Lu, Y., Luan, Y., Zhang, Z., Ding, J., Pan, D., 2025. Size fraction, behavior, and fate of trace metals along the river-estuary-coastal ocean continuum of Shandong peninsula, northern China. Mar. Environ. Res. 210. https://doi.org/10.1016/j.marenvres.2025.107324.

Miranda, L.S., Wijesiri, B., Ayoko, G.A., Egodawatta, P., Goonetilleke, A., 2021. Water-sediment interactions and mobility of heavy metals in aquatic environments. Water Res. 202. https://doi.org/10.1016/j.watres.2021.117386.

Mostafa, M.T., Nady, H.E., Gomaa, R.M., Abdelgawad, H.F., Farhat, H.I., Khalifa, I.H., Salman, S.A., 2023. Geochemical baseline and pre-mining environmental assessment of heavy metals at Iron exploration area. Northeastern Aswan, Egypt. Water Air and Soil Pollution 234 (7). https://doi.org/10.1007/s11270-023-06466-7.

Niazkar, M., Menapace, A., Brentan, B., Piraei, R., Jimenez, D., Dhawan, P., Righetti, M., 2024. Applications of XGBoost in water resources engineering: A systematic literature review. Environ. Model. Softw. 174. https://doi.org/10.1016/j.envsoft.2024.105971.

Parvin, A., Semme, S.A., Sultana, N., Moniruzzaman, M., Saha, B., al Mahmud, A., Hossain, M. K., 2025. Archival indicator of metal pollution in a tropical monsoon coastal region: impact on environment and human health. Mar. Pollut. Bull. 213. https://doi.org/10.1016/j.marpolbul.2025.117600.

Rubab, S., Khan, M.U., Mehboob, M., Malik, R.N., 2025. Spatial insights into microplastics and heavy metals levels, and risks in wastewater irrigated surface soils of Okara, Pakistan: microplastics sizes impacts on heavy metals distribution using structure equation model. Environ. Pollut. 368, 125786. https://doi.org/10.1016/j.envpol.2025.125786.

Sahoo, P.K., Guimaraes, J.T.F., Tyski, L., Reis, L.S., Leite, A.S., Gastauer, M., 2025. Exploring multi-media geochemical relationships in the southeastern Amazonian basin: A way forward to define source and background levels of potentially toxic elements in lake sediments. Environ. Res. 267. https://doi.org/10.1016/j.envres.2024.120648.

Salgado, J., Jaramillo-Monroy, C., Link, A., Lopera-Congote, L., Velez, M.I., Gonzalez-Arango, C., McGowan, S., 2025. Riverine connectivity modulates elemental fluxes through a 200-year period of intensive anthropic change in the Magdalena River floodplains. Colombia. Water Research 268. https://doi.org/10.1016/j.watres.2024.122633.

Santucci, L., Carol, E., Borda, L.G., García, M.G., 2024. Hydrochemistry and trace metals in water and sediments in forest coastal wetlands influenced by tidal regime in the middle río de la Plata estuary, argentina. Mar. Pollut. Bull. 202. https://doi.org/10.1016/j.marpolbul.2024.116359.

Song, H., Kim, T., Lee, J., Yoon, S.J., Kim, B., Kim, Y., Khim, J.S., 2025. Assessment of persistent toxic substances in sediments of Gyeonggi Bay, Korea: distributions, sources, and potential ecological risks. Mar. Pollut. Bull. 213. https://doi.org/10.1016/j.marpolbul.2025.117652.

Sun, Y., Yang, J., Li, K., Gong, J., Gao, J., Wang, Z., Lin, L., 2023. Differentiating environmental scenarios to establish geochemical baseline values for heavy metals in soil: A case study of Hainan Island. China. Science of the Total Environment 898. https://doi.org/10.1016/j.scitotenv.2023.165634.

Sun, Y., Sui, Q., Sun, J., Hou, Z., 2025. Historical record of trace elements since MIS 2 in a sediment core of Laizhou Bay, China. Environ. Monit. Assess. 197 (2). https://doi.org/10.1007/s10661-024-13607-w.

Taka, M., Aalto, J., Virkanen, J., Luoto, M., 2016. The direct and indirect effects of watershed land use and soil type on stream water metal concentrations. Water Resour. Res. 52 (10), 7711–7725. https://doi.org/10.1002/2016wr019226.

Tao, F., Tan, Y., Dai, J., Lu, C., Sha, Y., Liu, Y., Ma, Y., 2023. Occurrence of halogenated methanesulfonic acids in water and sediment from the Hangzhou Bay. China. Environmental Research 224. https://doi.org/10.1016/j.envres.2023.115463.

Tian, K., Wu, Q., Liu, P., Hu, W., Huang, B., Shi, B., Wang, T., 2020. Ecological risk assessment of heavy metals in sediments and water from the coastal areas of the Bohai Sea and the Yellow Sea. Environ. Int. 136. https://doi.org/10.1016/j.envint.2020.105512.

Tian, K., Liang, Q., He, Y., Ma, J., Zhao, T., Wu, Q., Teng, Y., 2024. Quantitative assessment of cd sources in rice grains through cd isotopes and MixSIAR model in a typical e-waste dismantling area of Southeast China. Sci. Total Environ. 954, 176217. https://doi.org/10.1016/j.scitotenv.2024.176217.

Ustaoglu, F., Yuksel, B., Yazman, M.M., Jaskula, J., Tokatli, C., 2025. Chemometric investigation of river system contamination: source identification and risk assessment using positive matrix factorization and Monte Carlo simulation. J. Contam. Hydrol. 273. https://doi.org/10.1016/j.jconhyd.2025.104627.

Wang, H., You, T., Gomez, M.A., Wang, Y., Li, S., Jia, Y., Shi, Z., 2021b. Chemical speciation and ecological risk assessment of cd, Pb and as in sediments: a case study in the Xijiang River basin. China. Environmental Earth Sciences 80 (12), 437. https://doi.org/10.1007/s12665-021-09724-1.

Wang, J., Chen, L., Song, Y., Li, Y., Liu, G., Yin, Y., Cai, Y., 2023. Adsorption and environmental behavior of mercury on the sediment from the Yellow Sea of China. J. Hazard. Mater. 443. https://doi.org/10.1016/j.jhazmat.2022.130333.

Wang, L., Liu, D., Sun, Y., Zhang, Y., Chen, W., Yuan, Y., Li, S., 2024. Machine learning-based analysis of heavy metal contamination in Chinese lake basin sediments: assessing influencing factors and policy implications. Ecotoxicol. Environ. Saf. 283. https://doi.org/10.1016/j.ecoenv.2024.116815.

Wang, L., Shi, G., Du, H., Zhang, J., Yao, L., Du, L., Pang, D., 2025a. From input to transformation: investigating the dynamic evolution of volatile organic compounds and driving mechanisms during sandstorms. Environ. Pollut. 374. https://doi.org/10.1016/j.envpol.2025.126192.

Wang, W., Huo, Y., Lin, C., Lian, Z., Wang, L., Liu, Y., Lin, H., 2024a. Occurrence, accumulation, ecological risk, and source identification of potentially toxic elements in multimedia in a subtropical bay, Southeast China. J. Hazard. Mater. 476. https://doi.org/10.1016/j.jhazmat.2024.135110.

Wang, X., Liu, X., Wu, H., Mi, T., Li, R., Zhang, C., 2021a. Interpretations of hg anomalous sources in drainage sediments and soils in China. J. Geochem. Explor. 224 (2021). https://doi.org/10.1016/j.gexplo.2020.106711.

Wang, Y., Zhang, J., Yan, Q., Guo, J., Liu, G., Hu, H., Zhao, Y., 2025b. Spatial distribution, sediment–water partitioning, risk assessment and source apportionment of heavy metals in the Golmud River-Dabson salt Lake ecosystem. Environ. Res. 268, 120792. https://doi.org/10.1016/j.envres.2025.120792.

Wang, Z., Bai, L., Zhang, Y., Zhao, K., Wu, J., Fu, W., 2022. Spatial variation, sources identification and risk assessment of soil heavy metals in a typical Torreya grandi cv.

Merrillii plantation region of southeastern China. Sci. Total Environ. 849. https://doi.org/10.1016/j.scitotenv.2022.157832.
Wang, Z., Li, X., Liu, X., Ding, R., Miao, C., 2024b. Understanding the environmental drivers of summer dissolved carbon in lakes on the Qinghai-Tibetan plateau. Sci. Total Environ. 951. https://doi.org/10.1016/j.scitotenv.2024.175720.
Wu, J., Wang, H., Han, Z., Shu, Y., Huang, X., Zhong, Q., Fan, Z., 2025b. Application of a PMF plus BMR hybrid model for source apportionment and ecological risk assessment of soil heavy metal(loid)s. J. Hazard. Mater. 494. https://doi.org/10.1016/j.jhazmat.2025.138734.
Wu, Q., Hu, W., Tian, K., Fan, Y.N., Khan, K.S., Hansen, H.C.B., Huang, B., 2025a. Quantification of sources and input-output pathways of heavy metals in soils from an abandoned mining watershed using cd isotope tracing and inventory analysis. Geoderma 459, 117359. https://doi.org/10.1016/j.geoderma.2025.117359.
Xiao, Z., Xie, X., Pi, K., Yan, Y., Li, J., Chi, Z., Wang, Y., 2018. Effects of irrigation-induced water table fluctuation on arsenic mobilization in the unsaturated zone of the Datong Basin, northern China. J. Hydrol. 564, 256–265. https://doi.org/10.1016/j.jhydrol.2018.07.018.
Xu, W., Gao, T., Wang, Z., Liu, Y., Liu, P., Tan, D., Liu, C., 2025. Experimental investigation of cadmium isotope fractionation during adsorption on montmorillonite and kaolinite. Environ. Sci. Technol. 59 (7), 3737–3748. https://doi.org/10.1021/acs.est.4c09245.
Yan, T., Wang, X., Liu, D., Chi, Q., Zhou, J., Xu, S., Wang, W., 2021. Continental-scale spatial distribution of chromium (Cr) in China and its relationship with ultramafic-mafic rocks and ophiolitic chromite deposit. Appl. Geochem. 126, 104896. https://doi.org/10.1016/j.apgeochem.2021.104896.
Yang, X., Lei, S., Zhao, Y., Cheng, W., 2022. Use of hyperspectral imagery to detect affected vegetation and heavy metal polluted areas: a coal mining area. China. Geocarto International 37 (10), 2893–2912. https://doi.org/10.1080/10106049.2020.1844308.
Yang, X., Ji, Y., Wang, B., Shi, J., Xu, W., Ma, J., Jiang, Y., 2025a. Status, sources and health risk assessment of PAHs, NPAHs and OPAHs in road dust of Xinjiang, China. Sci. Rep. 15 (1). https://doi.org/10.1038/s41598-025-99152-z.
Yang, Y., Qin, S., Li, Q., Wu, P., Li, X., 2025b. Study on the effects of Fe/Al on the distribution and fate of rare earth elements during the mixing of acid mine drainage with karst river water. J. Geochem. Explor. 277. https://doi.org/10.1016/j.gexplo.2025.107813.
Yin, R., Feng, X., Wang, J., Bao, Z., Yu, B., Chen, J., 2013. Mercury isotope variations between bioavailable mercury fractions and total mercury in mercury contaminated soil in Wanshan mercury mine, SW China. Chem. Geol. 336, 80–86. https://doi.org/10.1016/j.chemgeo.2012.04.017.
Zhang, H., Luo, Y., 2011. Endogenous and exogenous lead in soils of Yangtze River Delta region, China: identified by lead isotopic compositions and multi-elemental approaches. Environ. Earth Sci. 62 (5), 1109–1115. https://doi.org/10.1007/s12665-010-0599-y.
Zhang, L., Luo, M., Jiang, X., Tao, Y., Yang, D., Wang, L., Zang, L., 2025. Comprehensive assessment of biochar remediation performance for cadmium-contaminated sediment as affected by multiple physicochemical factors. Journal of environmental. Chem. Eng. 13 (3). https://doi.org/10.1016/j.jece.2025.116228.
Zhang, S., Li, Q., Zou, Y., Liu, B., Yang, J., Zheng, H., Liu, G., 2024. Using isotopic lead and strontium in sediments to trace natural and anthropogenic sources in the Bohai Sea. Sci. Rep. 14 (1). https://doi.org/10.1038/s41598-024-81493-w.
Zhao, L., Yan, Y., Yu, R., Hu, G., Cheng, Y., Huang, H., 2020. Source apportionment and health risks of the bioavailable and residual fractions of heavy metals in the park soils in a coastal city of China using a receptor model combined with Pb isotopes. Catena 194. https://doi.org/10.1016/j.catena.2020.104736.
Zhao, W., Ma, J., Liu, Q., Dou, L., Qu, Y., Shi, H., Wu, F., 2023. Accurate prediction of soil heavy metal pollution using an improved machine learning method: A case study in the Pearl River Delta. China. Environmental Science and Technology 57 (46), 17751–17761. https://doi.org/10.1021/acs.est.2c07561.
Zhao, Y., Zou, X., Liu, Q., Wang, C., Ge, C., Xu, M., 2018. Clay mineralogy indicates the muddy sediment provenance in the estuarine-inner shelf of the East China Sea. J. Asian Earth Sci. 152, 69–79. https://doi.org/10.1016/j.jseaes.2017.11.036.
Zhong, Q., Yin, M., Zhang, Q., Beiyuan, J., Liu, J., Yang, X., Zhang, Z., 2021. Cadmium isotopic fractionation in lead-zinc smelting process and signatures in fluvial sediments. J. Hazard. Mater. 411. https://doi.org/10.1016/j.jhazmat.2020.125015.
Zhou, W., Li, Z., Liu, Y., Shen, C., Tang, H., Huang, Y., 2024b. Soil type data provide new methods and insights for heavy metal pollution assessment and driving factors analysis. J. Hazard. Mater. 480, 135868. https://doi.org/10.1016/j.jhazmat.2024.135868.
Zhou, Y., Du, S., Liu, Y., Yang, T., Liu, Y., Li, Y., Zhang, L., 2024a. Source identification and risk assessment of trace metals in surface sediment of China Sea by combining APCA-MLR receptor model and lead isotope analysis. J. Hazard. Mater. 465. https://doi.org/10.1016/j.jhazmat.2023.133310.
Zhuang, W., Ying, S.C., Frie, A.L., Wang, Q., Song, J., Liu, Y., Lai, X., 2019. Distribution, pollution status, and source apportionment of trace metals in lake sediments under the influence of the south-to-north water transfer project, China. Sci. Total Environ. 671, 108–118. https://doi.org/10.1016/j.scitotenv.2019.03.306.

Tracing threats across the land−marine transition areas: Decoding heavy metal sources and risks in soil-water-sediment systems of northern and eastern coastal China

Qiumei Wu [a, b, c], Peng Liu [d], Shiyi Zhang [a], Guojing Yan [a], Kang Tian [a], Wenyou Hu [a, b, c *], Tieyu Wang [e], Jong Seong Khim [f], Seongjin Hong [g], Bong-Oh Kwon [h], Ya'nan Fan [a], Biao Huang [a, b]

Affiliations

[a] *State Key Laboratory of Soil and Sustainable Agriculture, Institute of Soil Science, Chinese Academy of Sciences, Nanjing 211135, China*

[b] *Sino-Danish College, University of Chinese Academy of Sciences, Beijing, 100049, China*

[c] *Sino-Danish Center for Education and Research (SDC) , Beijing, 100049, China*

[d] *College of Resources and Environment, Anqing Normal University, Anqing, 246011, China*

[e] *Institute of Marine Sciences, Shantou University, Shantou 515063, China*

[f] *School of Earth and Environmental Sciences, Research Institute of Oceanography, Seoul National University, Seoul 08826, Republic of Korea*

[g] *Department of Marine Environmental Sciences, Chungnam National University, Daejeon 34134, Republic of Korea*

[h] *Department of Marine Biology, Kunsan National University, Kunsan 54150, Republic of Korea*

1

[*]**Corresponding author.**
Address: State Key Laboratory of Soil and Sustainable Agriculture, Institute of Soil Science, Chinese Academy of Sciences, Nanjing 211135, China. Tel.: +86 25 86881268; fax: +86 25 876881000. *E-mail address*: wyhu@issas.ac.cn (W. Hu)

Contents

Figure lists

Table lists

Text S1 Measurement process of Cd and Pb isotopes

At the three sampling sites (Fig. S1), soil, sediment, rice, and atmospheric deposition samples were collected for Cd isotope analysis (Wu et al., 2025; Tian et al., 2024), while at sites (a) and (b), various agricultural system media were additionally sampled for Pb isotope analysis (Liu et al., 2023). The detailed isotopic analysis procedure is presented in Figs. S2 and S3. The reference isotopic values were obtained from the literature (Chae et al., 2014; Chrastný et al., 2018; Munksgaard et al., 2000; Sakata et al., 2018; Shen et al., 2023; Yao et al., 2015; Zhang et al., 2024).

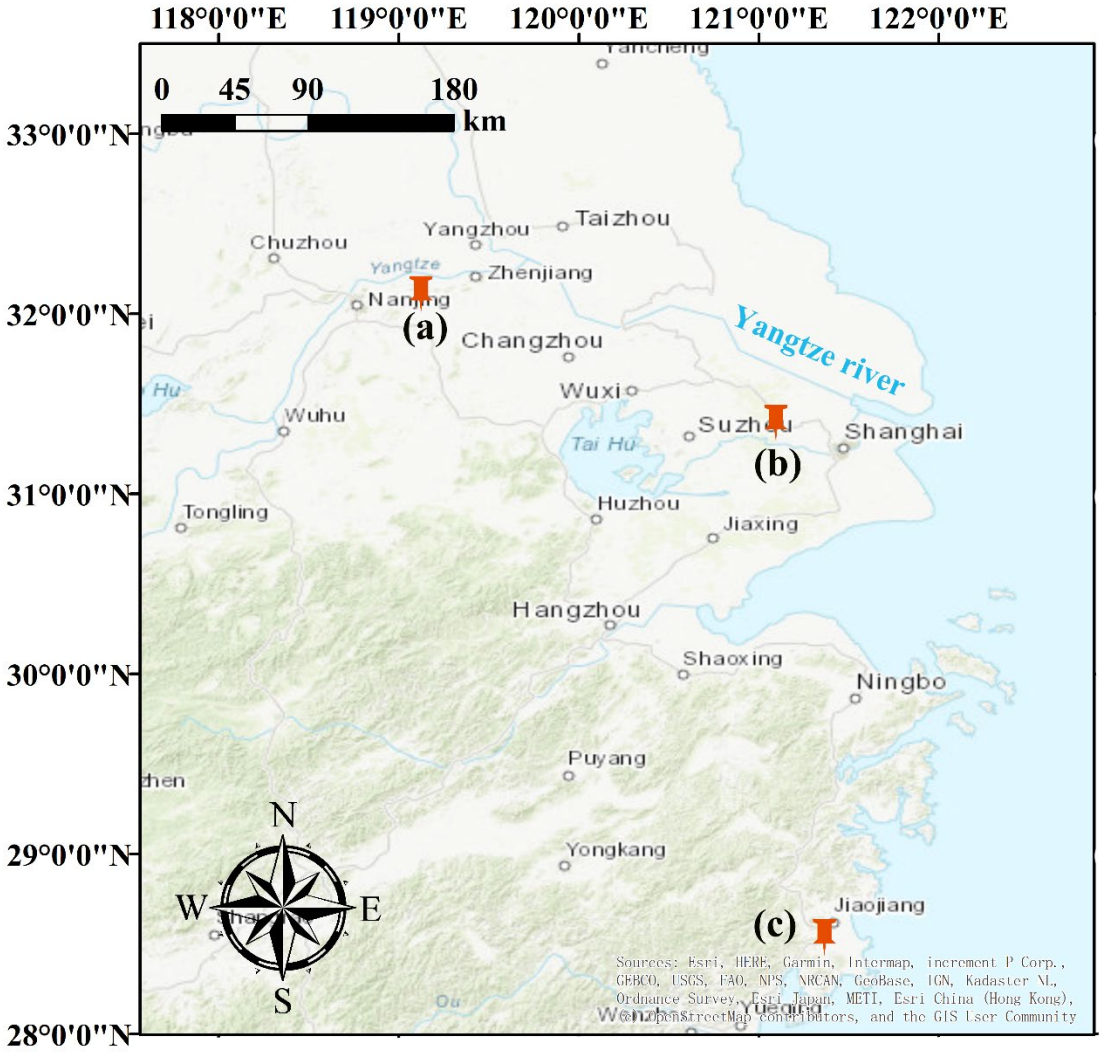

Fig.S1. Spatial distribution of isotope monitoring sites in the study area. (a) Historical mining watershed in the upper Yangtze River. (b) A representative rapidly developing economic region at the Yangtze River estuary. (c) Modernized port city in the Yangtze River Delta (YRD).

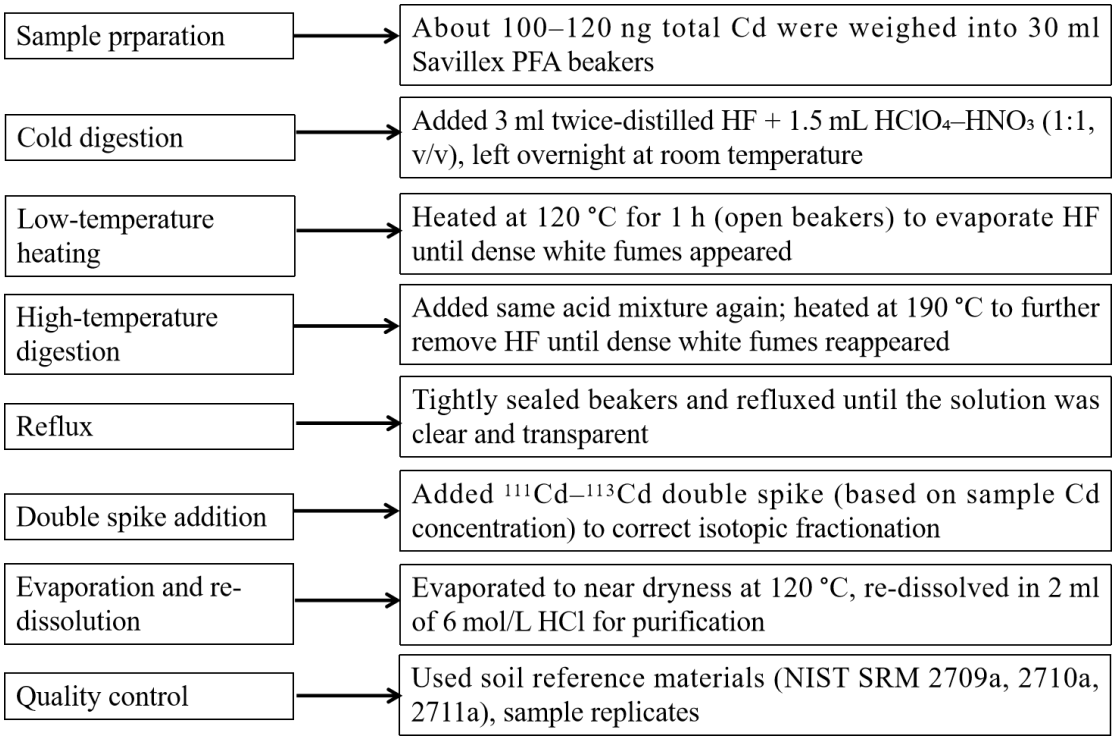

Fig.S2. The analytical process of Cd isotopes

$$\delta_{Soil} = f_{Atmos}\delta_{Atmos} + f_{Background}\delta_{Background} \quad (1\text{-}1)$$

$$1 = f_{Atmos} + f_{Background} \quad (1\text{-}2)$$

where $f_{Atmos}$and $f_{Background}$ represent the contributions of atmospheric deposition and the background soil layer to the surface soil heavy metal content, respectively. δ_{Soil}, δ_{Atmos}, and $\delta_{Background}$represent the $^{206}Pb/^{207}Pb$ ($^{208}Pb/^{206}Pb$) ratios in surface soil, atmospheric deposition, and background soil, respectively.

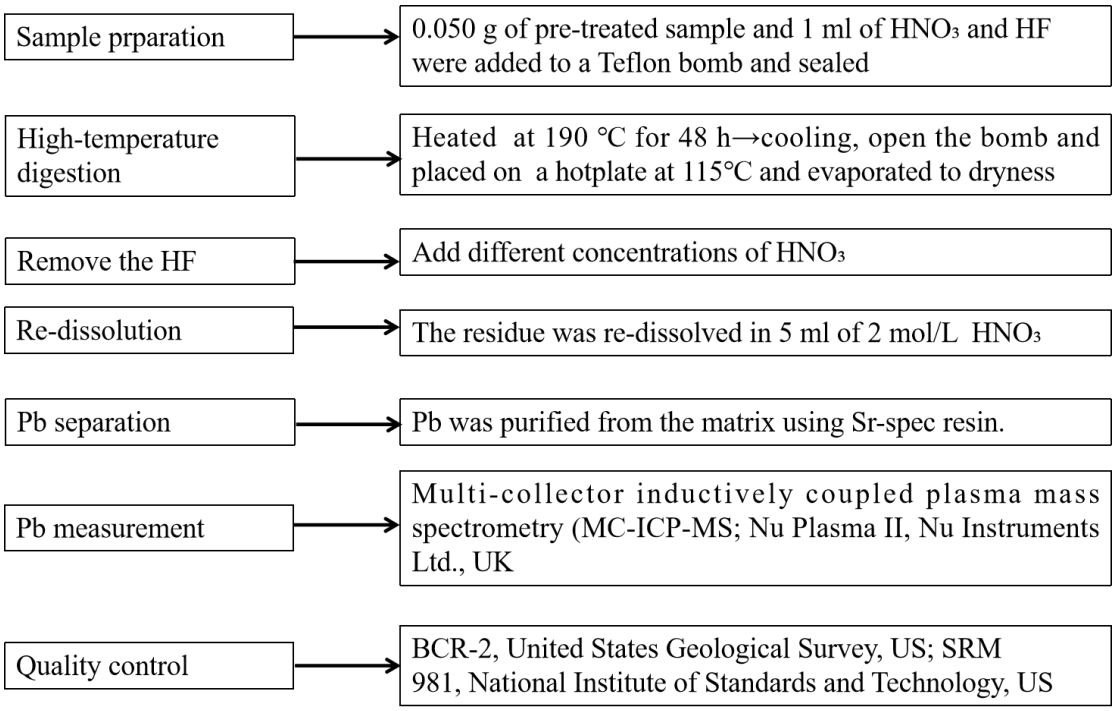

Fig.S3. The analytical process of Pb isotopes

Cd isotopic compositions are reported as $\delta^{114/110}$Cd (‰) relative to the NIST SRM 3108 standard, calculated according to the following equation (Yao et al., 2024):

$$\delta^{114/110}\text{Cd} = \left[\frac{(114_{Cd}/110_{Cd})_{sample}}{(114_{Cd}/110_{Cd})_{NIST\ 3108}} - 1\right] \times 1000 \quad (1\text{-}3)$$

The "apparent" isotopic fractionation between components A and B was calculated through the following equation:

$$\Delta^{114/110}\ Cd_{A-B} = \delta^{114/110}Cd_A - \delta^{114/110}Cd_B \quad (1\text{-}4)$$

To quantify the sources of Cd and Pb in surface soils, both an end-member model and a Bayesian mixing model were applied. In the Bayesian framework, a Dirichlet (1,1,1) prior was used to constrain the source proportions (ensuring non-negativity and a total sum of one). The likelihood function was constructed by treating the observed Cd concentrations and isotopic ratios as normally distributed perturbations of the weighted combination of endmembers. Markov Chain Monte Carlo (MCMC) sampling was employed to obtain the posterior distributions of the contributions from the three endmembers, with the mean values and 95% credible intervals reported. Detailed computational procedures are provided in Wu et al. (2025) and Liu et al. (2023).The correlation equation is as follows:

$$X_{i,j} \sim N\left(\sum_k p_k(\mu_{j,k} + \lambda_{jk}), \sum_k pk^2(\omega_{jk}{}^2 + \tau_{jk}{}^2)\right) \quad (1\text{-}5)$$

Where $X_{i,j}$ represents the trace value j of the mixture i, the isotopic value of the sample; p_k represents the proportion of source k, $\mu_{j,k}$ is the mean of source k for tracer j; λ_{jk} is mean discrimination factor which can be replaced by fractionation value; ${\omega_{jk}}^2$ is the discrimination factor for source k variance for tracer j; τ_{jk} is the discrimination factor variance for tracer j on source k.

Table S1 Cadmium concentrations (mg/kg) and isotope compositions (‰) in different media

Sample type	Cd concentration (mg/kg)	$\delta^{114/110}$Cd (‰)	Sample size (N)
Surface soil	1.81 ± 0.94	0.04 ± 0.10	14
Atmospheric deposition	1.65 ± 0.68	-0.26 ±0.08	5
Deep soil	0.36 ± 0.27	-0.07 ± 0.27	8
Sediment	9.33 ± 10.59	-0.04 ± 0.13	7
Water	0.083 ± 0.13	0.22 ± 0.26	5
Rice	0.59 ± 0.64	0.26 ± 0.19	11

Note: Mean (± standard deviation, SD) Cd concentrations (mg/kg) and isotopic compositions ($\delta^{114/110}$Cd, ‰) in different environmental media

Table S2 Lead (Pb) concentrations (mg/kg) and isotope compositions (‰) in different media

Sample type	$^{206/207}$ Pb	$^{208/206}$ Pb	Location
Surface soil	1.17±0.013	2.09±0.013	This study
Atmospheric deposition	1.16±0.007	2.10±0.011	This study
Deep soil	1.19±0.014	2.08±0.013	This study
Sediment	1.18±0.003	2.10±0.009	This study
Coal	1.13	2.14	Chae et al., 2014
Traffic emission dust	1.156	2.103	Shen et al., 2023
Factory emission dust	1.166	2.095	Shen et al., 2023
Coal fly ash	1.155	2.118	Shen et al., 2023

Text S2 Structural equation model (SEM)

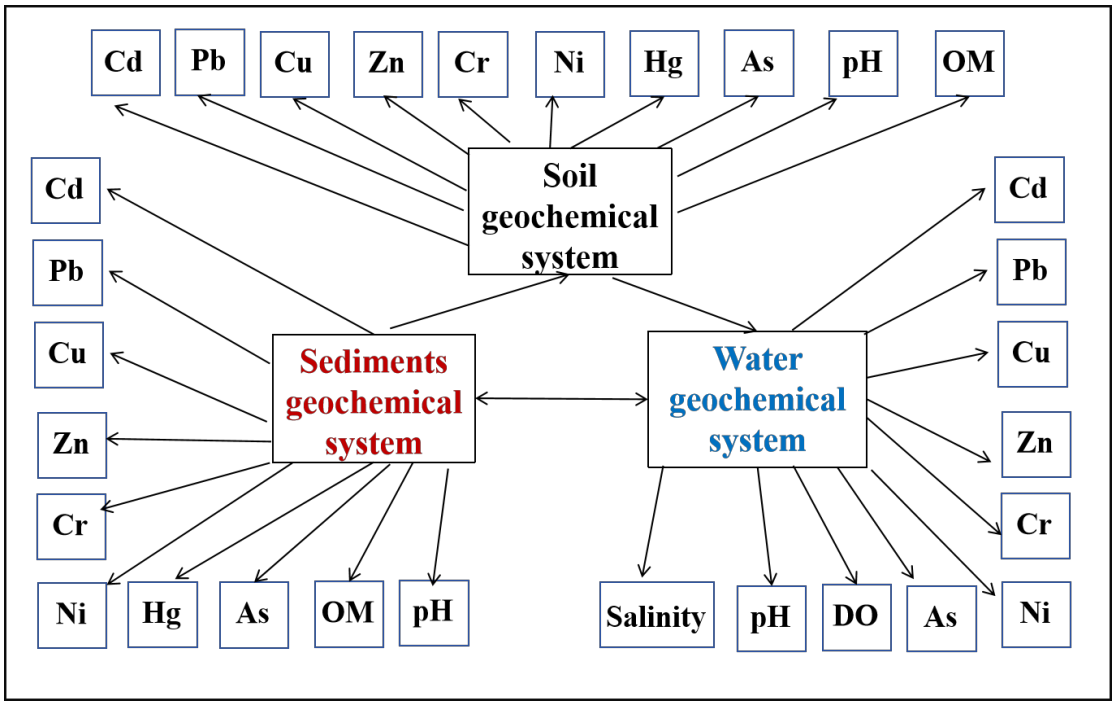

Fig.S4. Conceptual framework for the structural equation model (SEM)

Structural equation modeling (SEM) was employed to investigate the relationships among latent and observed variables (Kondo et al., 2024). SEM integrates factor analysis and path analysis within a unified framework, allowing simultaneous estimation of measurement errors, direct effects, and indirect effects. The SEM framework consists of two submodels: the measurement model and the structural model (Grace et al., 2010). The measurement model specifies the relationships between latent variables and their corresponding observed indicators as:

$$x = \Lambda_x \xi + \delta \quad (2\text{-}1)$$

$$y = \Lambda_y \eta + \varepsilon \quad (2\text{-}2)$$

Where x and y are the vectors of exogenous and endogenous observed variables, respectively. ξ and η represent the exogenous and endogenous latent variables. Λ_x and Λ_y are factor loading matrices. δ and ε denote measurement errors associated with x and y, respectively.

The structural model describes the causal relationships among latent variables:

$$\eta = B\eta + \Gamma\xi + \zeta \quad (2\text{-}3)$$

where B is the matrix of coefficients representing the relationship among endogenous latent variables, Γ represents the effects of exogenous latent variables on

endogenous latent variables, and ζ denotes the structural disturbances

Table S3 Model fit indices for the structural equation model.

Fit Index	Value
Degrees of freedom	105
Comparative Fit Index (CFI)	0.960
Tucker-Lewis Index (TLI)	0.952
Root Mean Square Error of Approximation (RMSEA)	0.036
RMSEA 90% CI (lower)	0.000
RMSEA 90% CI (upper)	0.067
P-value H_0: RMSEA ≤ 0.05	0.732
P-value H_0: RMSEA ≥ 0.08	0.007
Standardized Root Mean Square Residual (SRMR)	0.076

Text S3 Positive matrix factorization (PMF)

The positive matrix factorization (PMF) model is a multivariate receptor model used for source apportionment of heavy metals (Joe et al., 2025). PMF decomposes the measured heavy metal concentration matrix X into a factor contribution matrix G and a factor profile matrix F. By repeatedly applying the least-squares method to decompose X, the optimal G and F matrices are obtained, and the target function Q is minimized to achieve source identification. The computational procedure is as follows:

$$X_{ij}=\sum_{k=1}^{P}(g_{ik}f_{kj}+e_{ij}) \quad (2\text{-}1)$$

$$Q=\sum_{i=1}^{n}\sum_{j=1}^{m}(\frac{e_{ij}}{u_{ij}})^2 \quad (2\text{-}2)$$

$$u_{ij}=\sqrt{(S\times C_s)^2+(0.5\times MDL)^2} \quad (2\text{-}3)$$

$$u_{ij}=\frac{5}{6}\times MDL \quad (2\text{-}4)$$

The model diagnostics further confirmed the robustness of the PMF results. The Q(Robust)/Q(True) values were 1.30 for soil and 1.39 for sediment, both within the recommended EPA range of 1–2, indicating good agreement between observed and predicted data. Bootstrap analysis (150 runs) demonstrated stable factor mapping across 100% of runs, and the relative change in Q(Robust) was 24.8% for soil and 29.4% for sediment, suggesting stable and reproducible source contributions. In addition, less than 3% of samples exhibited residuals beyond ±3σ (Table S2); these samples were retained to preserve dataset representativeness but were automatically down-weighted in robust mode, minimizing their impact on the final solution.

Table S4 Key diagnostic parameters of the PMF model for soil and sediment datasets

Parameters	Soil	Sediment	Explanation
Q (Robust)	1113.3	1179.2	Objective function under robust mode
Q (Ttue)	859.4	850.1	Theoretical objective function
Q (Robust)/Q (True)	1.30	1.39	Model fit indicator; within the acceptable EPA range (1–2), and predicted data
dQ (Robust)	276.5	347.1	Change in robust Q
% dQ (Robust)	24.8%	29.44%	Relative uncertainty, reflecting stability of the solution
Q (Aux)	257.7	329.29	Auxiliary Q value, confirming robustness of factor profiles
Convergence	Yes	Yes	Model successfully converged
Outliers (Residuals > ±3σ)	< 3%	< 3%	Less than 17 samples

Text S4 *Identification of Key Environmental Drivers via XGBoost*

The potential ecological risk index (PERI) was calculated separately for soil and surface sediment samples using a revised Hakanson method

$$PERI = \sum_{i=1}^{n} E_r^i = \sum_{i=1}^{n} T_r^i C_f^i \quad (3\text{-}1)$$

where E_r^i represent potential ecological risk factor for metal i. T_r^i denotes toxic response factors of metal i. C_f^i stand for contamination factor for metal i.

All predictor variables X_j were standardized as:

$$x_j' = \frac{x_j - u_j}{\sigma_j} \quad (3\text{-}2)$$

Where x_j represents the original feature value, u_j is the mean, and σ_j is the

standard deviation of valuable j. This transformation centers the data around zero and scales it to unit variance, thereby facilitating efficient model training and improving the numerical stability of the algorithm.

Model training and feature selection, initial models were trained using XGBoost to compute feature importance scores (Miller et al., 2023). Based on the ranked importance from XGBoost, the top 10 predictors were selected to construct the final regression models. The final model $f(\mathrm{x})$ is an ensemble of K regression trees:

$$\hat{y}_i = f(x_i) = \sum_{k=1}^{K} f_k(X_i),\ f_k \in \mathcal{F} \quad (3\text{-}3)$$

where $\mathcal{F}$ denotes the space of regression trees.

Table S5 Input and target variables in this study

Variable types	Influence factors	PERI_soil	PERI_sediments	Data source
Pollution and migration factors	CF (contamination factor of 8 HMs)	✓	-	This study
	Kd (The partition coefficientsof 7 HMs in soil-sediment	-	✓	This study
Physical and chemical property factors	pH/OM	✓		This study
	Salinity		✓	This study
Geographical and natural factors	NDVI	✓	✓	A
	Lithology	✓	✓	B
	DEM	✓	✓	C
Human factor	Enterprise_density	✓	✓	B
	POP	✓	✓	A
	GDP	✓	✓	A
	Land use type	✓	✓	A
Meteorological	PRE_total	✓	✓	A

factor	TEM_avr	✓	✓	A

Note: A signify data from the Resource and Environment Science Data platform (https://www.resdc.cn/). B indicates data obtained from Sayre et al. (2014). C present Geographic elevation information was sourced from the digital elevation model (DEM) provided by the National Spatial Data Infrastructure Portal (http://www.nsdi.go.kr).

Text S5 Other informations

Table S6 Summary of advantages and limitations of four statistical approaches for GeoBs estimation

Methods	Advantages	Limitation	Suitability
Iterative mean method[a]	Simple to implement; widely used in geochemical mapping	Sensitive to extreme values; may underestimate GeoBs in anthropogenically influenced datasets	Useful for initial baseline estimates, but less robust in heterogeneous coastal zones
Iterative median method[b]	Robust against outliers and skewed distributions; provides stable and conservative estimates	Slightly underestimate in multi-modal distributions	Highly suitable for heterogeneous coastal environments with mixed natural and anthropogenic inputs
Relative cumulative frequency method[c]	Identifies inflection points in skewed/multi-modal distributions	Often yields higher thresholds, potentially masking moderate pollution	Applicable in estuarine and transition zones, but prone to overestimation
Boxplot method[d]	Non-parametric; independent of distributional assumptions	Oversimplifies variability; sensitive to dataset size	Useful as a supplementary benchmark in coastal settings

Note: The baseline estimation methods for a, b, c, and d followed those described by Zhang et al. (2020), Reimann et al. (2005), Xian et al. (2022), and Huang et al. (2024), respectively.

Table S7 Regional background values of heavy metal(loid)s in coastal soils and

sediments of China ((Literature compilation)

Region	As	Cd	Cr	Cu	Hg	Ni	Pb	Zn
				Soil[a]				
Liaoning	8.80	0.11	57.90	19.80	0.04	25.60	21.40	63.50
Hebei	13.60	0.09	68.30	21.80	0.04	30.80	21.50	78.40
Tianjin	9.60	0.09	84.20	28.80	0.08	33.30	21.00	79.30
Shandong	9.30	0.08	66.00	24.00	0.02	25.80	25.80	63.50
Jiangsu	10.00	0.13	77.80	22.30	0.29	26.70	26.20	62.60
Mean	10.26	0.10	70.84	23.34	0.094	28.44	23.18	69.46
				Sediment				
Bohai sea[b]	10.0	0.136	60.0	17.54	0.030	36.1	11.29	55.3
Yellow sea of China[c]	5.40	0.103	45.2	15.64	0.0158	21.6	14.15	58.0
Mean	7.70	0.12	52.6	16.59	0.023	28.85	12.72	56.65

[a]: the background values of heavy metals in **soils** in the different areas of China were cited from CNEMC (1990). [b]: The BS data of background values of **sediments** are cited from Zhang et al. (2011) and Duan and Li, 2017. [c]: The YSC data of background values are cited from Lu and Zhu (1987) and Li et al. (2017a).

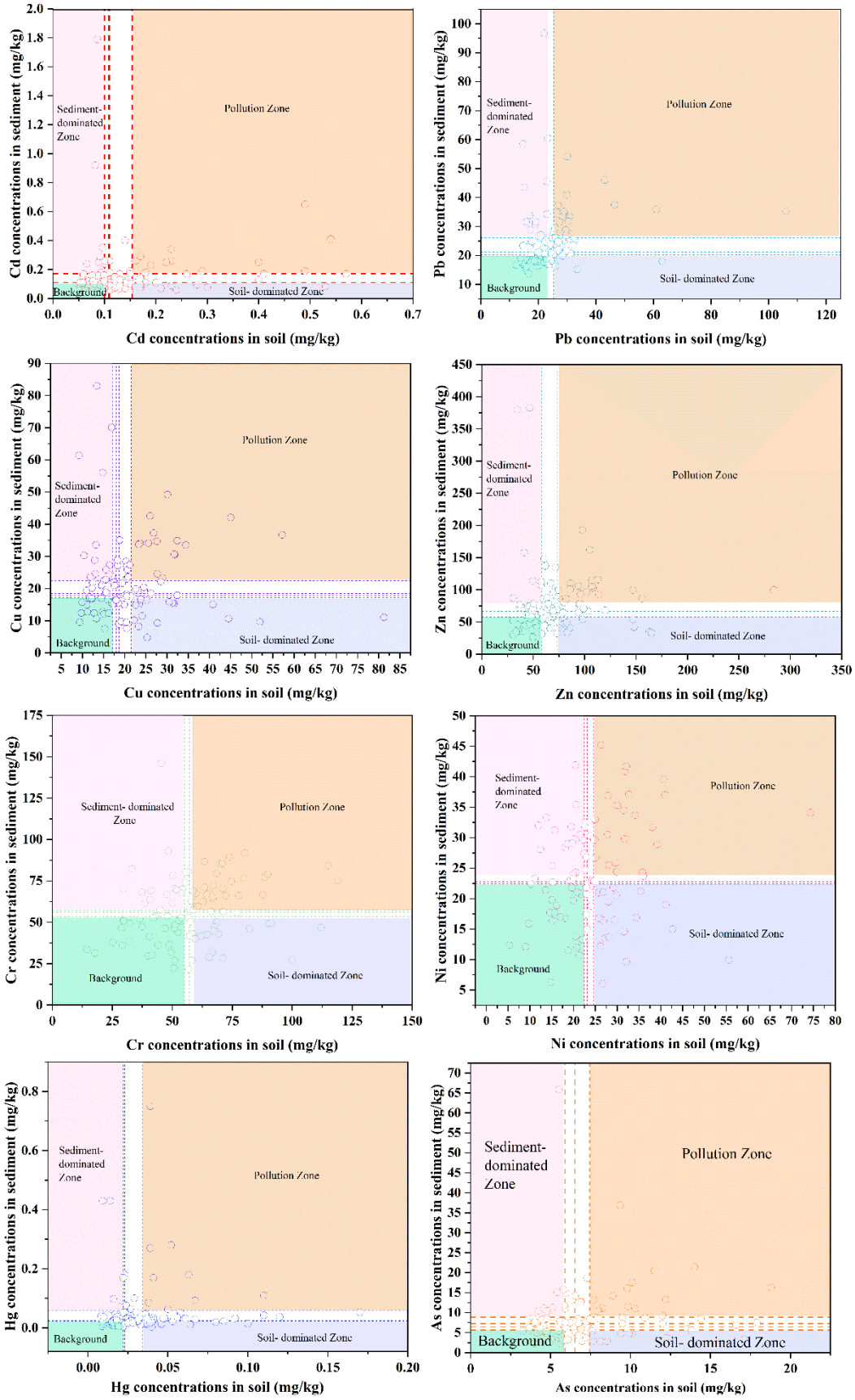

Fig.S5. GeoBs-based concentration–risk zoning of heavy metals in soils and sediments. The Background Zone represents concentrations below the minimum GeoB values determined by the

four statistical methods. The Soil-dominated and Sediment-dominated Zones correspond to cases where concentrations fall between the lowest GeoB value of one medium and the highest GeoB value of the other. The Pollution Zone indicates sites where both soil and sediment concentrations simultaneously exceed their respective maximum GeoB values, representing dual-media contamination.

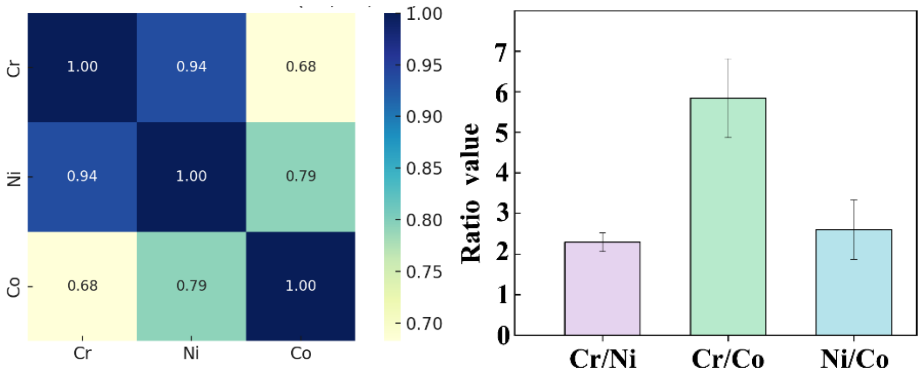

Fig.S6. Correlation analysis and percentage box plot of stable elements in sediments from the Yangtze River estuary

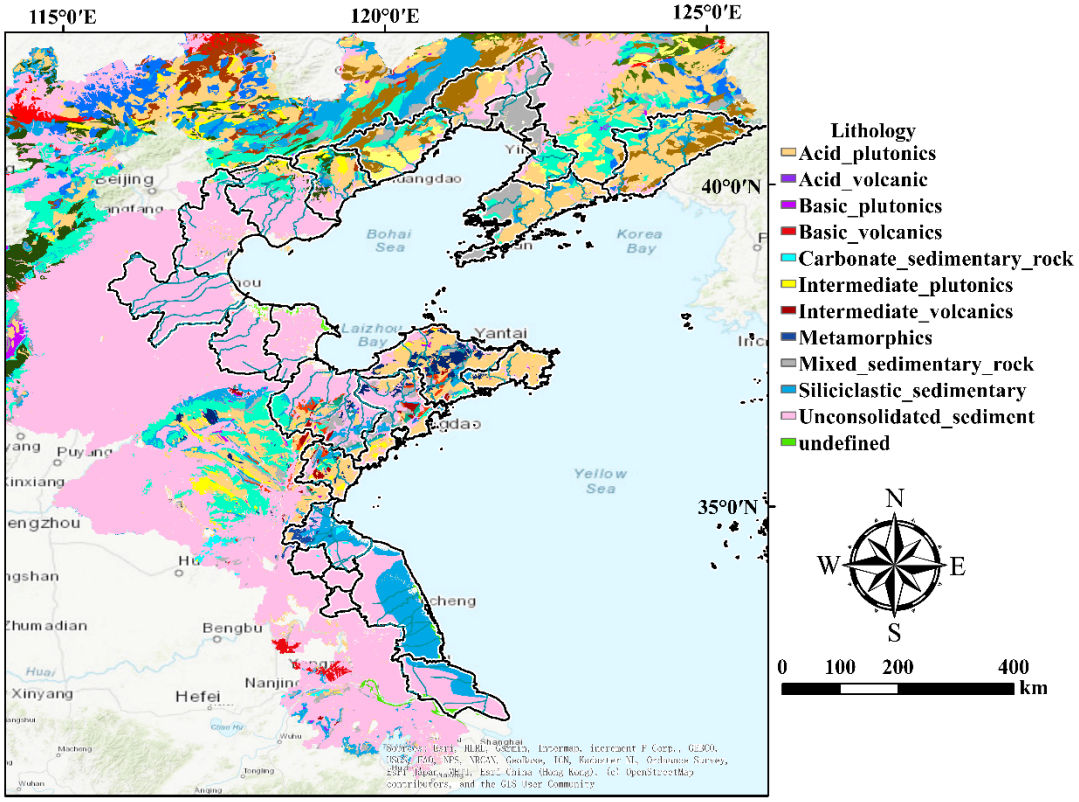

Fig.S7. A spatial distribution map of the dominant lithologies in the study area. The lithological data used in this study were derived from Sayre et al. (2014).

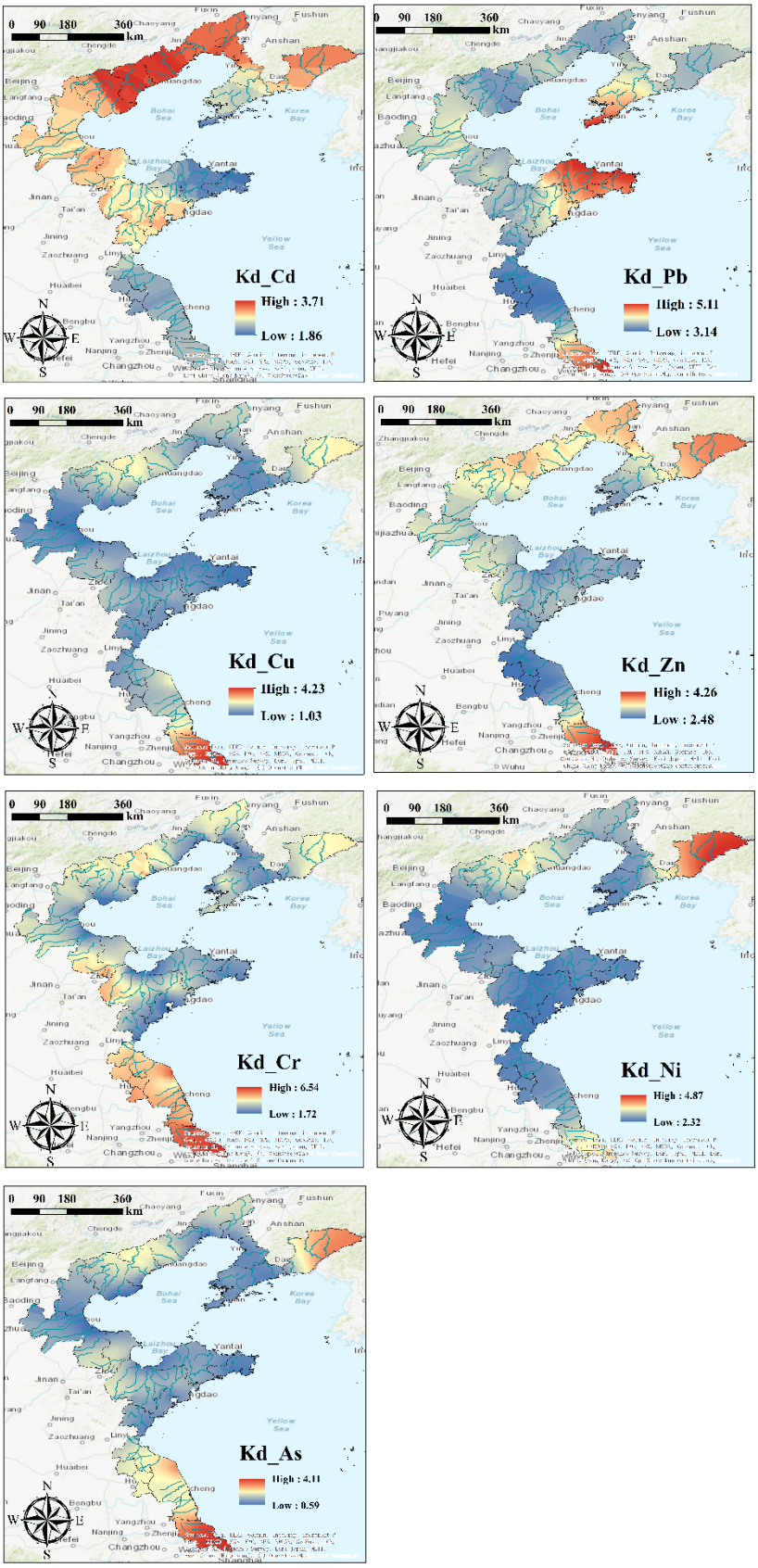

Fig.S8. The spatial distribution of the partition coefficient (K_d) of heavy metals between sediment and water

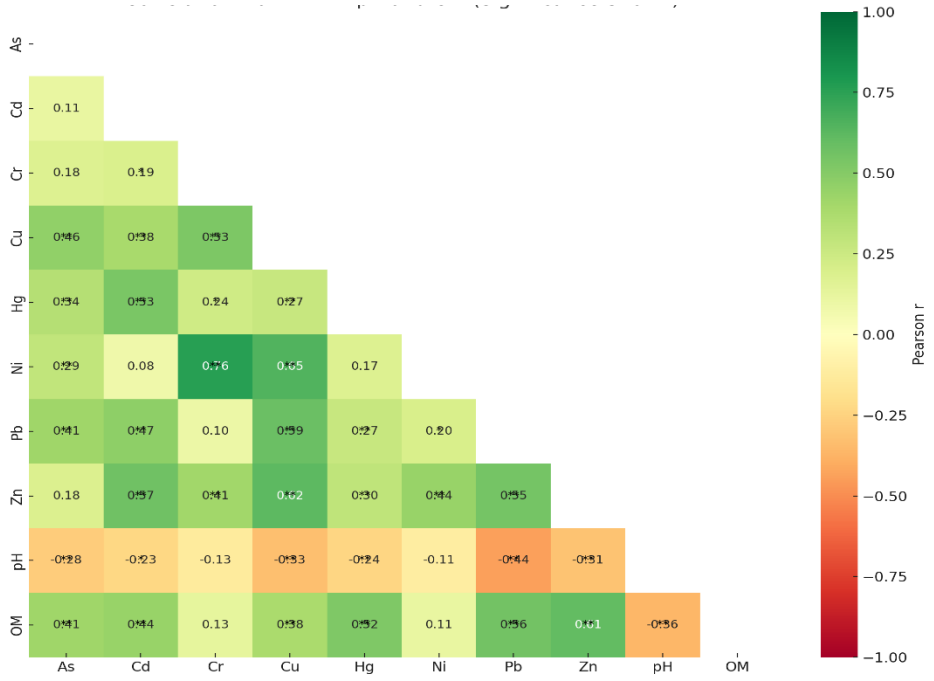

Fig.S9. Pearson correlation coefficients between soil heavy metal concentrations and physicochemical properties.

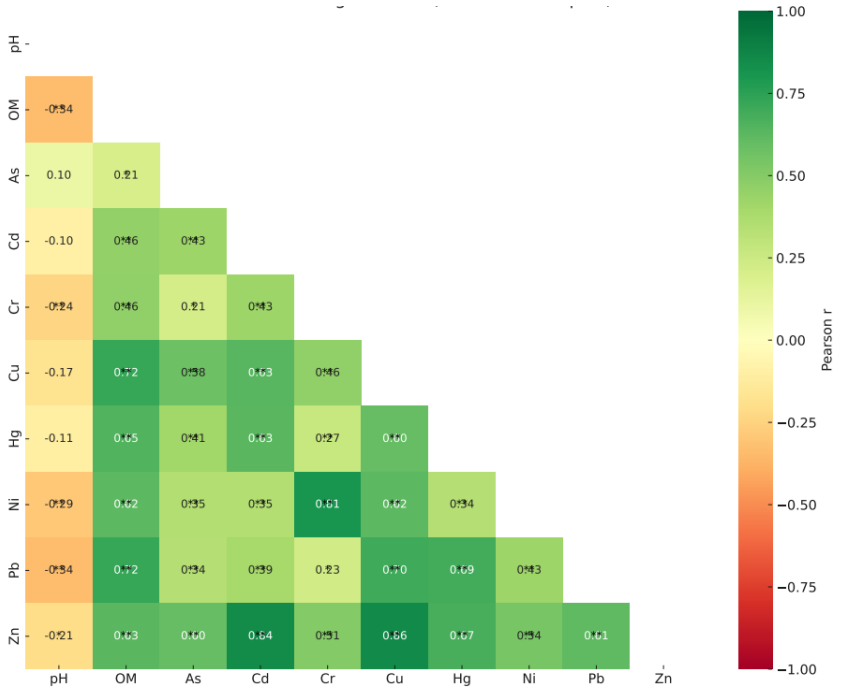

Fig.S10. Pearson correlation coefficients between sediment heavy metal concentrations and physicochemical properties.

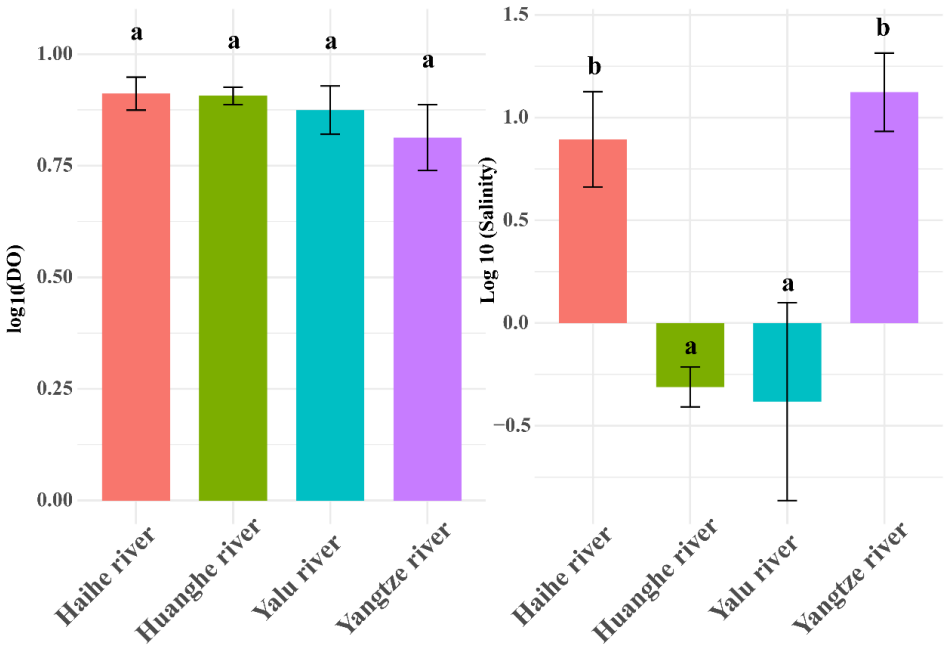

Fig.S11. Comparative analysis of dissolved oxygen and Salinity (log10-transformed) across four rivers

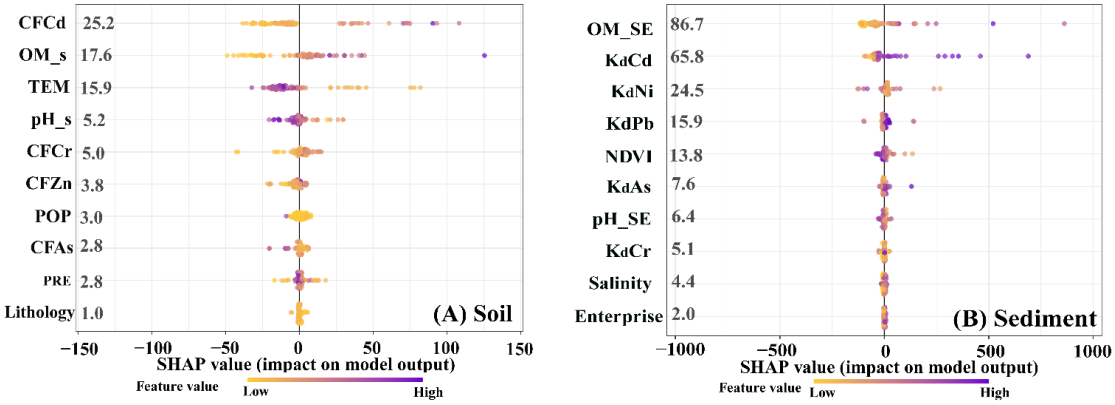

Fig.S12. Prediction of the PERI of HMs in soil (A) and sediments (B) with XGBoost

Table S8 Terminology used to describe the risk factors E_r^i and R_I as suggested by Håkanson (1980)

E_r^i	Potential ecological risk for single regulator	R_I	Ecological risk for all factors
$E_r^i < 40$	Low	$R_I < 100$	Low
$40 \leqq E_r^i < 80$	Moderate	$100 \leqq R_I < 200$	Moderate
$80 \leqq E_r^i < 160$	Considerable	$200 \leqq R_I < 400$	Considerable
$160 \leqq E_r^i < 320$	High	$R_I \geqq 400$	Very High
$E_r^i \geqq 320$	Very High		

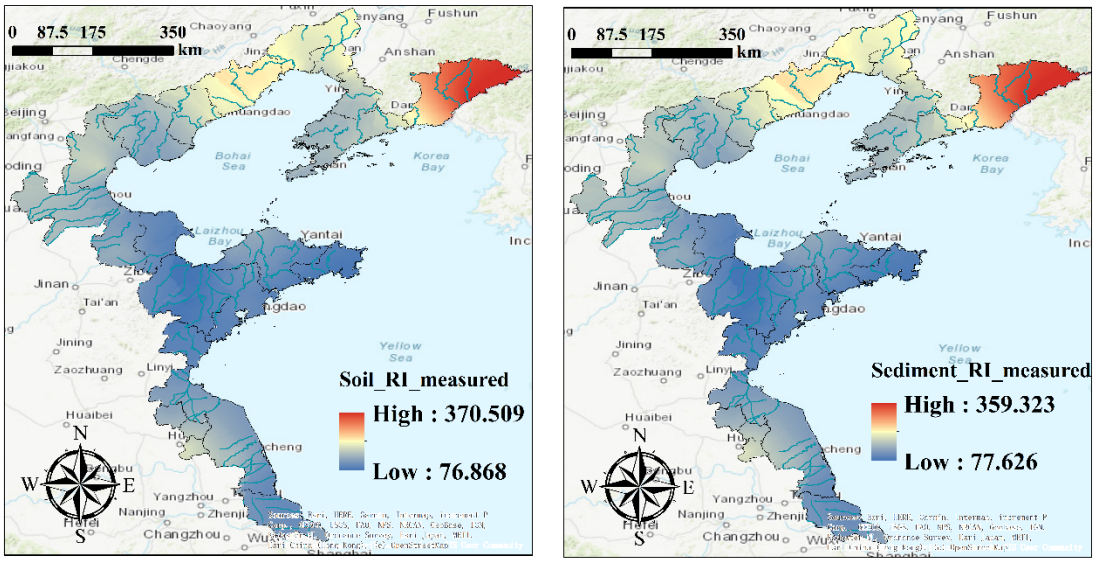

Fig.S13. Spatial distribution of predicted ecological risk index (PERI) for soil and sediment in the coastal region

To apportion sources of Pb and Cd in surface soils, isotope-based mixing models were applied. For Pb, a two-endmember framework was constructed with parent material and atmospheric deposition as sources, using $^{206}Pb/^{207}Pb$ and $^{208}Pb/^{206}Pb$ ratios. Deterministic calculations were performed for each ratio, followed by a Bayesian model jointly constrained by both isotopes to obtain posterior means and 95% credible intervals. For Cd, three sources were considered (parent material, atmospheric deposition, and fertilizer), combining Cd concentrations with $\delta^{114/110}Cd$ values. Both deterministic linear mixing and a Bayesian Dirichlet–Gaussian framework were used to derive source contributions and uncertainty bounds. Results are summarized in Table S7, showing that Bayesian estimates were consistent with deterministic means while providing credible intervals that quantify uncertainty.

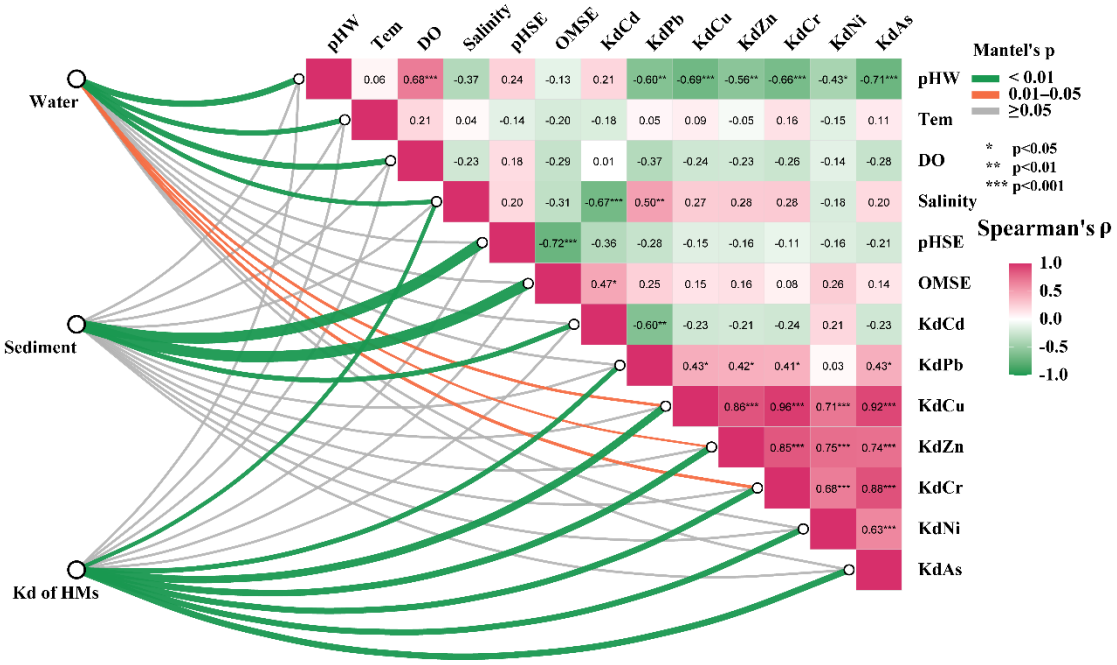

Fig.S14. Spearman correlation matrix of heavy metal partition coefficients (Kd) and environmental variables, with Mantel test linkages.

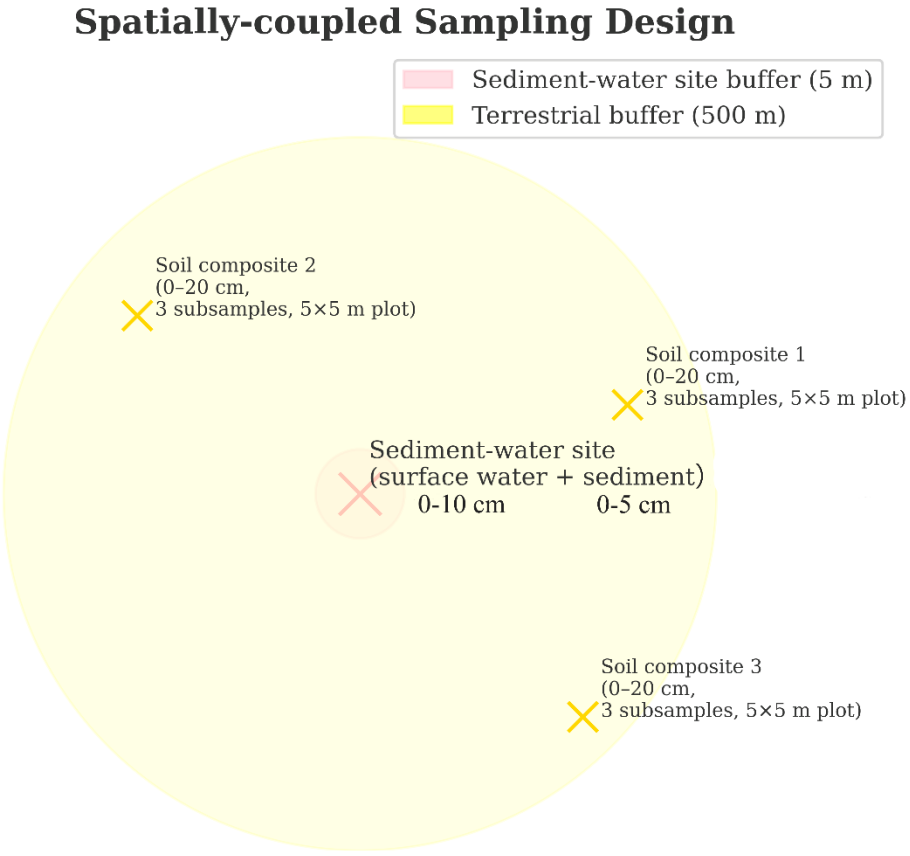

Fig.S15. Spatially coupled soil–sediment–water sampling design

Fig.S16. Field investigation and sampling of soil, sediment, and water

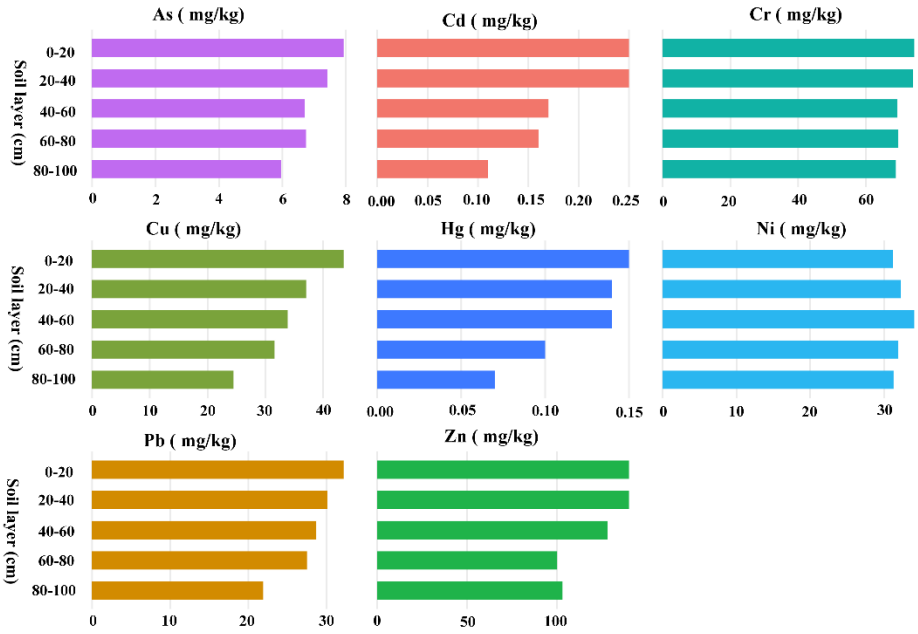

Fig.S17. The distribution of heavy metals in soil profiles around the Yangtze River estuary

(Unpublished data)

Table S9 Multiple regression model identifying key drivers of Cd partitioning coefficient

Variable	Coefficient (β)	Std. Error	t-value	p-value
const	324.359	171.073	1.90	0.073
pHW	-4.795	17.291	-0.28	0.785
Temp(℃)	-6.534	2.223	-2.94	0.008
DO	1.807	2.620	0.69	0.499
Salinity	-0.946	0.375	-2.52	0.021
pHSE	-11.411	19.145	-0.60	0.558
OMSE	1.111	0.800	1.39	0.181

Note: R-squared: 0.651, F-statistic: 5.91, p = 0.001.

Table S10 Multiple regression model identifying key drivers of Ni partitioning coefficient

Variable	Coefficient (β)	Std. Error	t-value	p-value
pHW	-6857.908	3961.785	-1.73	0.100
Temp(℃)	-6857.908	3961.785	-1.73	0.100
DO	-1031.880	509.256	-2.03	0.057
Salinity	-103.645	85.996	-1.21	0.243
pHSE	6004.564	4386.612	1.37	0.187
OMSE	199.878	183.335	1.09	0.289

Note: R-squared: 0.31, F-statistic: 1.39, p = 0.26.

References

Chae, J. S., Choi, M. S., Song, Y. H., Um, I. K., Kim, J. G. (2014). Source identification of heavy metal contamination using metal association and Pb isotopes in Ulsan Bay sediments, East Sea, Korea. *Marine pollution bulletin, 88(1-2), 373-382.* doi: 10.1016/j.marpolbul.2014.07.066

Chrastný, V., Šillerová, H., Vítková, M., Francová, A., Jehlička, J., Kocourková, J., Komárek, M. (2018). Unleaded gasoline as a significant source of Pb emissions in the Subarctic. *Chemosphere, 193, 230-236*. doi:10.1016/j.chemosphere.2017.11.031

Duan, X., Li, Y. (2017). Distributions and sources of heavy metals in sediments of the Bohai Sea, China: a review. *Environmental Science and Pollution Research, 24(32), 24753-24764*. doi:10.1007/s11356-017-0330-6

Grace, J. B., Anderson, T. M., Olff, H., Scheiner, S. M. (2010). On the specification of structural equation models for ecological systems. *Ecological monographs, 80(1), 67-87*. doi: 10.1890/09-0464.1

Huang, H., Chai, Y., Xu, C., Lei, J., Guo, F. (2024). Determination and Applicability Analysis of Heavy Metal Geochemical Baseline in Farmland: A Case Study of a County in the Upper Reaches of the Xihan River. *Earth and Environment. 2025,53(04):546-555*. doi: 10.3724/EE.1672-9250.2024.52.057 (Chinese)

Joe, D. J., Choi, M. S., Lee, J. H., Kim, C. K. (2025). Identifying mining and smelting contributions to metal contamination in lake and river sediments, South Korea. *Environmental Earth Sciences, 84(15), 430*. doi:10.1007/s12665-025-12439-2

Kondo, M., Korre, A., Komai, T., Watanabe, N. (2024). Multi-layered physical factors govern mercury release from soil: Implications for predicting the environmental fate of mercury. Journal of Environmental Management, 352, 120024. doi:10.1016/j.jenvman.2024.120024

Li, H., Liu, Y., Cheng, Y., 2017a. Background values of heavy metals in the sediments of Yalu River estuary and its adjacent coasts. *Environmental Chemistry, 36, 1047–1055* (In Chinese).

Liu, P., Wu, Q., Hu, W., Tian, K., Huang, B., Zhao, Y. (2023). Comparison of heavy metals in riverine and estuarine sediments in the lower Yangtze River: Distribution, sources, and ecological risks. Environmental Technology and Innovation, 30, 103076. doi:10.1016/j.eti.2023.103076

Lu, S.Y., Zhu, M.Y., 1987. The background value of chemical elements in the Huanghai Sea sediment. Acta Oceanolog. Sin. 6, 558–567 (In Chinese).

Miller, T., Kozlovska, P., Krzemińska, A., Lewita, K., Biedrzycka, J., Geroch, K. (2023) XGBoost in environmental ecology: a powerful tool for sustainable insights. doi:10.36074/grail-of-science.08.12.2023.33

Munksgaard, N. C., Parry, D. L. (2000). Anomalous lead isotope ratios and provenance of offshore sediments, Gulf of Carpentaria, northern Australia. *Australian Journal of Earth Sciences, 47(4), 771-777*. doi:10.1007/s10872-017-0448-7

Reimann, C., Filzmoser, P., & Garrett, R. G. (2005). Background and threshold: critical comparison of methods of determination. *Science of the total environment, 346(1-3), 1-16*. doi:10.1016/j.scitotenv.2004.11.023

Sakata, M., Xu, H., Mashio, A. S. (2018). Analysis of historical trend of pollution sources of lead in Tokyo Bay based on lead isotope ratios in sediment core. *Journal of Oceanography, 74(2), 187-196.* doi:10.1007/s10872-017-0448-7

Sayre, R., J. Dangermond, C. Frye, R. Vaughan, P. Aniello, S. Breyer, D. Cribbs, D. Hopkins, R. Nauman, W. Derrenbacher, D.Wright, C. Brown, C. Convis, J. Smith, L. Benson, D. Paco VanSistine, H. Warner, J. Cress, J. Danielson, S. Hamann, T. Cecere, A. Reddy, D. Burton, A. Grosse, D. True, M. Metzger, J. Hartmann, N. Moosdorf, H. Dürr, M. Paganini, P. DeFourny, O. Arino, S. Maynard, M. Anderson, and P. Comer, 2014, A New Map of Global Ecological

Land Units – An Ecophysiographic Stratification Approach. Washington, DC: Association of American Geographers. 46 pages.

Shen, Y. W., Zhao, C. X., Zhao, H., Dong, S. F., Xie, J. J., Lv, M. L., Yuan, C. G. (2023). Decryption analysis of antimony pollution sources in PM2. 5 through a multi-source isotope mixing model based on lead isotopes. *Environmental Pollution, 328, 121600*. doi:10.1016/j.envpol.2023.121600

Tian, K., Wu, Q., Liu, P., Hu, W., Huang, B., Shi, B., Wang, T. (2020). Ecological risk assessment of heavy metals in sediments and water from the coastal areas of the Bohai Sea and the Yellow Sea. *Environment International, 136*. doi:10.1016/j.envint.2020.105512

Wu, Q., Hu, W., Tian, K., Fan, Y. N., Khan, K. S., Hansen, H. C. B., Huang, B. (2025). Quantification of sources and input-output pathways of heavy metals in soils from an abandoned mining watershed using Cd isotope tracing and inventory analysis. *Geoderma*, *459, 117359*. doi:10.1016/j.geoderma.2025.117359

Xian, H., Dong, X., Wang, Y., Li, Y., Xing, J., Jeppesen, E. (2022). Geochemical baseline establishment and pollution assessment of heavy metals in the largest coastal lagoon (Pinqing Lagoon) in China mainland. *Marine Pollution Bulletin*, *177*, 113459. doi:10.1016/j.marpolbul.2022.113459

Yao, C., Yang, Y., Li, C., Shen, Z., Li, J., Mei, N., Wang, D. (2024). Heavy metal pollution in agricultural soils from surrounding industries with low emissions: Assessing contamination levels and sources. *Science of the Total Environment, 917*. doi:10.1016/j.scitotenv.2024.170610

Yao, P. H., Shyu, G. S., Chang, Y. F., Chou, Y. C., Shen, C. C., Chou, C. S., Chang, T. K. (2015). Lead isotope characterization of petroleum fuels in Taipei, Taiwan. *International journal of environmental research and public health, 12(5), 4602-4616*. doi: 10.3390/ijerph120504602

Zhang, H., Yu, M., Xu, H., Wen, H., Fan, H., Wang, T., Liu, J. (2020). Geochemical baseline determination and contamination of heavy metals in the urban topsoil of Fuxin City, China. *Journal of Arid Land, 12(6), 1001-1017*. doi:10.1007/s40333-020-0029-2

Zhang, L., Yanwen, Q.I.N., Binghui, Z., Jing, J.I.A., Kun, L.E.I., 2011. Distribution and pollution assessment of heavy metals in sediments from typical areas in the Bohai Sea. *Acta Scientiae Circumstantiae 31, 1676–1684*. (In Chinese).

Zhang, S., Li, Q., Zou, Y., Liu, B., Yang, J., Zheng, H., Liu, G. (2024). Using isotopic lead and strontium in sediments to trace natural and anthropogenic sources in the Bohai Sea. *Scientific Reports, 14(1), 30267*. doi:10.1038/s41598-024-81493-w